THE UNIVERSITY OF ALBERTA

A DEVICE FOR POINT SOURCE SIMULATION IN A HIGH FREQUENCY ACOUSTICAL SYSTEM

BY

© JOHN D. W. KETTLEWELL

A THESIS

SUBMITTED TO THE FACULTY OF GRADUATE STUDIES AND RESEARCH

IN PARTIAL FULFILMENT OF THE REQUIREMENTS FOR THE DEGREE

OF MASTER OF SCIENCE

DEPARTMENT OF ELECTRICAL ENGINEERING

EDMONTON, ALBERTA

SPRING, 1972

THE UNIVERSITY OF ALBERTA

FACULTY OF GRADUATE STUDIES AND RESEARCH

The undersigned certify that they have read, and recommend to the Faculty of Graduate Studies and Research, for acceptance, a thesis entitled "A Device For Point Source Simulation In A High Frequency Acoustical System" submitted by John D. W. Kettlewell in partial fulfilment of the requirements for the degree of Master of Science.

ABSTRACT

A technique utilizing a piezoelectric disc and a liquid filled exponential horn combination for the generation and detection of ultrasound is described.

The experimental results, which are consistent with theoretical predictions, indicate that these devices can be used to closely simulate the radiation profile of point sources or receivers.

The data also suggest that these transducer-horn units can be conveniently employed as elements in the newer "crossed-array" acoustical holographic systems.

ACKNOWLEDGMENTS

The work described in this thesis was carried out in the Department of Electrical Engineering, University of Alberta, under the supervision of Dr. H. J. J. Seguin and Dr. H. G. Schmidt-Weinmar, to whom the author is very grateful for both advice and encouragement received throughout the course of this project.

Acknowledgment is also extended to the workshop for construction of the experimental apparatus, and to Mr. R. A. Schmaus for the design of electronic circuitry and electronic supplies.

Gratitude for the financial support received from the National Research Council of Canada and the Department of Electrical Engineering is expressed.

ACKNOWLEDGMENTS

The work described in this thesis was carried out in the Department of Electrical Engineering, University of Alberta, under the supervision of Dr. H. J. J. Seguin and Dr. H. G. Schmidt-Weinmar, to whom the author is very grateful for both advice and encouragement received throughout the course of this project.

Acknowledgment is also extended to the workshop for construction of the experimental apparatus, and to Mr. R. A. Schmaus for the design of electronic circuitry and electronic supplies.

Gratitude for the financial support received from the National Research Council of Canada and the Department of Electrical Engineering is expressed.

TABLE OF CONTENTS

FIGURE CAPTIONS

CHAPTER 1

INTRODUCTION

In recent years acoustics has enjoyed rapidly growing popularity in scientific research. The increased activity in this area is largely due to the many new and imaginative uses that scientists and engineers are finding for ultrasonic vibrations [1]. Medical people are using echograms as a method of forming images of the interior anatomy. Materials scientists are investigating ways of utilizing ultra-sound for non-destructive testing. In the field of optical communications acoustic waves are used to amplitude and frequency modulate laser light. As a last example probably the most exciting research in acoustics has been in the new field of acoustic holography.

Because of the many uses for ultra-sonic vibrations much attention has been directed towards acoustic radiators and detectors. For instance a recent publication describes the design of an ultrasonic generator for the treatment of Meniere's disease[2]. This thesis describes a device which may be used as either a point source receiver or a point source transmitter.

Conventional spherical radiators of ultra-sound in water are usually made of a piezoelectric ceramic which operates in a thickness resonance mode [3]. The shape of the radiator which is that of a spherical surface segment serves two purposes. Firstly the large area provides a method of coupling a sufficient amount of acoustic power into the water and secondly the concave radiating

surface results in focusing of the acoustic radiation to simulate a point source radiator.

The device described in this thesis consists of a piezoelectric disc which radiates into a horn of exponentially decreasing cross-section. The disc provides the large area required for coupling sufficient energy into the water while the horn serves to focus the radiation to closely simulate a point source. This device is reversible and may be used as a sensitive non-directional point receiver.

In many respects the piezoelectric disc-horn device described in this thesis is superior to the more conventional acoustic transducers as will become apparent later in this thesis.

CHAPTER 2

DEVICE DESCRIPTION

2.1 Physical details

The device shown photographically in figure [1] and schematically in figure [2] consists of an acoustic transducer mounted in a liquid filled horn. The transducer is piezoelectric, it is one centimeter in diameter and operates in the thickness mode with the resonant frequency being one megahertz. The horn is made of copper and has an exponentially decreasing radial cross-section. Fabrication of these horns was achieved by electroforming copper onto a stainless steel mandrel. Appendix [A] contains electroforming details.

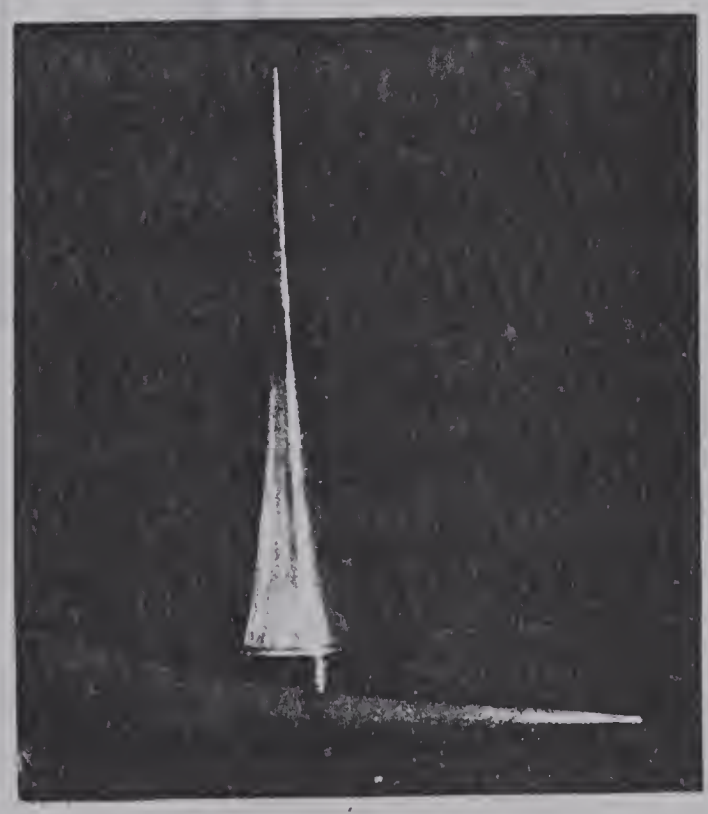

FIGURE 1

Photograph of electroformed copper horn and stainless steel mandrel

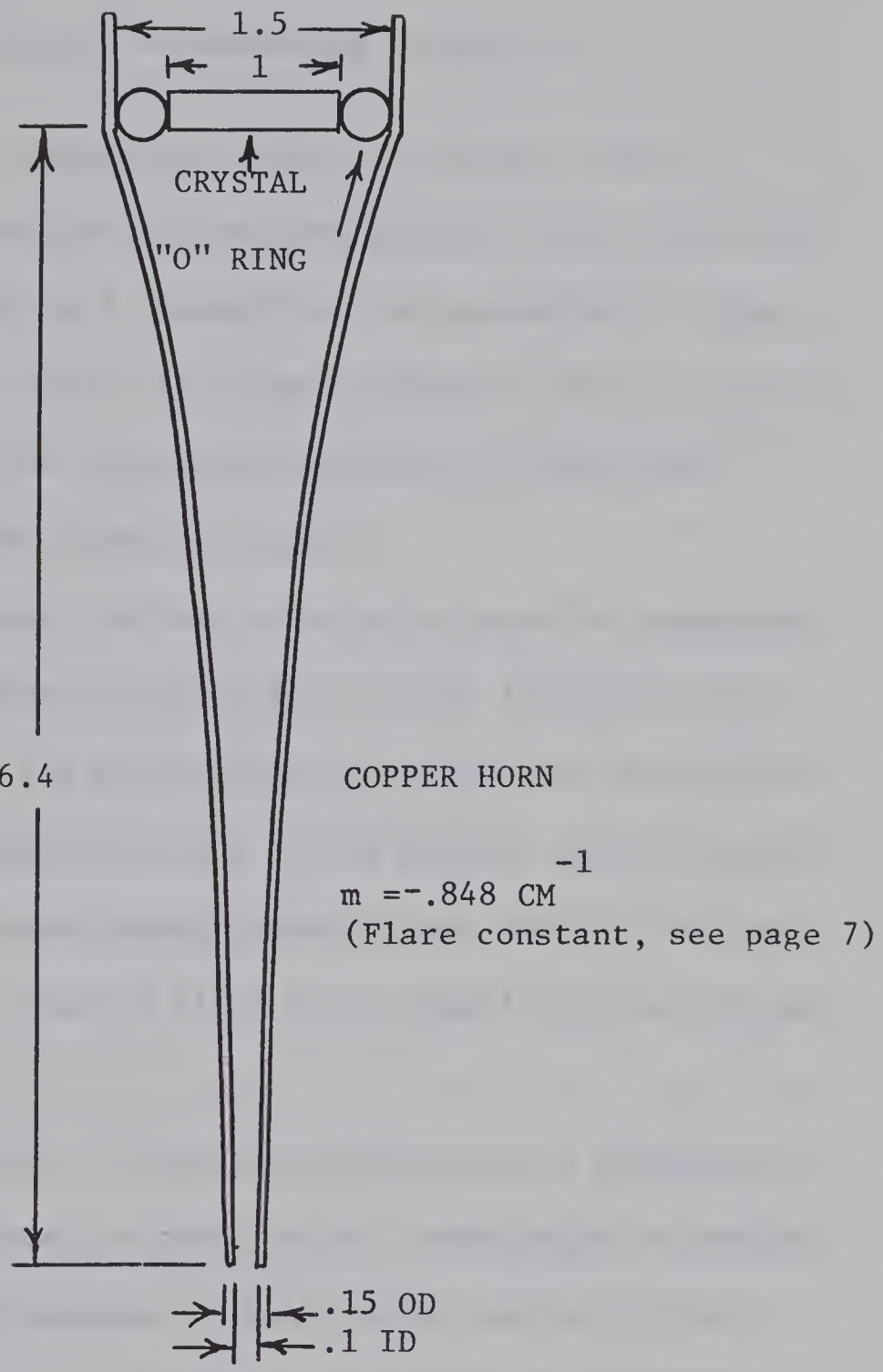

Dimensions in centimeters

FIGURE [2] pzt-horn details

2.2 Qualitative description of operating principles

The piezoelectric transducer which is located in the large end of the copper horn can perform either of two functions. When the device is used as a transmitter the piezoelectric disc transforms electrical power into acoustic power or when the device is used as a receiver the transducer delivers an electrical signal from the received acoustic signal.

Because of its shape the horn acts as an acoustic impedance transformer. The impedance seen by the crystal is that of the radiation impedance of the small aperture of the horn multiplied by the ratio of the transducer area to the smaller aperture area. It is this impedance transforming property that enables the horn to achieve an intense acoustic field at the small aperture of the horn.

The smaller aperture of the horn illustrated in figure [2] is, for the frequency used, a fraction of a wavelength in radius. This aperture closely simulates either a point source of high intensity or a point receiving element over a limited field of view.

The small aperture and the flexible character of the thin copper horn make it possible to create an array of several point

receivers very close together. This array fabrication is accomplished by bending of the acoustic waves in a manner analogous to the way in which light waves are bent via fiber optics.

Very recently W. Wells introduced a new acoustic holographic system which he calls the "multi-element linear crossed array" [4]. This system promises to alleviate many of the problems found in conventional holographic methods [5, 6, 7].

The sources and receivers to be used in such a holographic system must be spaced not more than one or two wavelengths apart [8]. This constraint had previously limited Wells' system to long wavelength holography where it is relatively easy to make transducers which radiate a reasonsable amount of power from an aperture of radius of less than one wavelength. The aforementioned properties of the piezoelectric horn device meet the requirements of the holographic system proposed by Wells so that the crossed array system has now become feasible for frequencies of one megahertz and perhaps as high as ten megahertz.

CHAPTER 3

THEORETICAL DISCUSSION

3.1 Mathematical treatment of horn

The theoretical analysis of horns which have exponentially increasing radial cross-sections has been adequately treated in the literature [9, 10, 11]. Section 3.1 follows closely reference [9]. Analysis of horns of exponentially decreasing cross-section is identical with the exception that the flare constant is negative.

The cross-section of the horn is given by:

$$S = S_1 e^{mx}$$

$$m = \frac{\partial \ln S}{\partial x}$$

S_1 = cross-sectional area at x = 0

S = cross-sectional area

m = flare constant

Assuming that the waves incident on the horn are plane and that the phase and amplitude remain constant on a plane normal to the horn axis as the wave propogates down the horn then the velocity potential is shown in appendix B to be:

$$\phi = (A'e^{u_1 x} + B'e^{u_2 x})e^{i\omega t}$$

ϕ = velocity potential

$$u_1 = -\frac{m}{2} + \frac{i}{2}\sqrt{4k^2 - m^2} = -\alpha + i\beta$$

$$u_2 = -\frac{m}{2} - \frac{i}{2}\sqrt{4K^2 - m^2} = -\alpha - i\beta$$

ω = frequency in radians per second

k = wave number = $\frac{2\pi}{\lambda}$

λ = wavelength

The velocity and excess pressure are obtained from the velocity potential as:

(1) $\dot{\xi} = e^{-\alpha x}(Ae^{-i(\beta x + \theta)} - Be^{i(\beta x + \theta)})e^{i\omega t}$

(2) $p = \rho_o c e^{-\alpha x}(Ae^{-i\beta x} + Be^{i\beta x})e^{i\omega t}$

$\dot{\xi}$ = particle velocity

p = excess pressure

ρ_o = medium density

c = velocity of sound in medium

$\theta = \tan^{-1}\frac{\alpha}{\beta}$

Note that the constants A and B are not the constants A' and B' which appear in the expression for ϕ. Equations (1) and (2) are

written so that they may be easily compared to plane waves. It is noted that there is a phase difference between $\dot{\xi}$ and p which does not occur in plane waves. Note also that $\dot{\xi}$ and p increase in amplitude exponentially with x.

Knowledge of the impedance at both ends of the horn allows the determination of the constants A and B. For a horn which is terminated at x = 0 with a piston impedance Z_o and at x = ℓ with Z_ℓ the equations of force at the boundaries are:

(3) at x = 0 $\quad Z_o \dot{\xi}_1 + p_1 S_1 = \psi e^{i\omega t}$

Z_o = piston impedance at the front of the horn

$\psi e^{i\omega t}$ = the driving force

(4) at x = ℓ $\quad Z_\ell \dot{\xi}_2 - p_2 S_2 = 0$

ℓ = length of horn

Z_ℓ = the complex impedance which terminates the horn.

From equations (1), (2) and (4):

$$B = Ae^{-i2\beta\ell} \left\{ \frac{Z_\ell e^{-i\theta} - \rho_o c S_2}{Z_\ell e^{i\theta} + \rho_o c S_2} \right\}$$

Now by using (3) we have:

$$A = \left\{ \frac{Z_\ell e^{i\theta} + \rho_o c S_2}{2De^{-i\beta\ell}} \right\} \psi$$

Hence:

$$B = e^{-i\beta\ell}\left\{\frac{Z_\ell e^{-i\theta} - \rho_o c S_2}{2D}\right\}\psi$$

$$2D = (Z_o Z_\ell + \rho_o{}^2 c^2 S_1 S_2)(e^{i\beta\ell} - e^{-i\beta\ell})$$
$$+ \rho_o c\{Z_o S_2(e^{i(\beta\ell - \theta)} + e^{-i(\beta\ell - \theta)})$$
$$+ Z_\ell S_1(e^{i(\beta\ell + \theta)} + e^{-i(\beta\ell + \theta)})\}$$

$$D = (Z_o Z_\ell + \rho_o^2 c^2 S_1 S_2) i \sin[\beta\ell]$$
$$+ c\rho_o\{Z_\ell S_1 \cos[\beta\ell + \theta] + Z_o S_2 \cos[\beta\ell - \theta]\}$$

The expressions for $\dot{\xi}$ and p become:

$$p = \frac{\rho_o c e^{-\alpha x}}{D}\{\rho_o c S_2 i \sin[\beta(\ell - x)] + Z_\ell \cos[\beta(\ell - x) + \theta]\}\psi e^{i\omega t}$$

$$\dot{\xi} = \frac{e^{-\alpha x}}{D}\{Z_\ell i \sin[\beta(\ell - x)] + \rho_o c S_2 \cos[\beta(\ell - x) - \theta]\}\psi e^{i\omega t}$$

An equivalent "T" network for the horn is developed by considering the horn to have inertia coefficients L_1, M and L_2 just as a transformer.

In electrical engineering, systems containing four variables that are uniquely determined when two of the variables are known are called two port networks. There are many ways in which such networks may be represented, one of which is known as the equivalent "T" network.

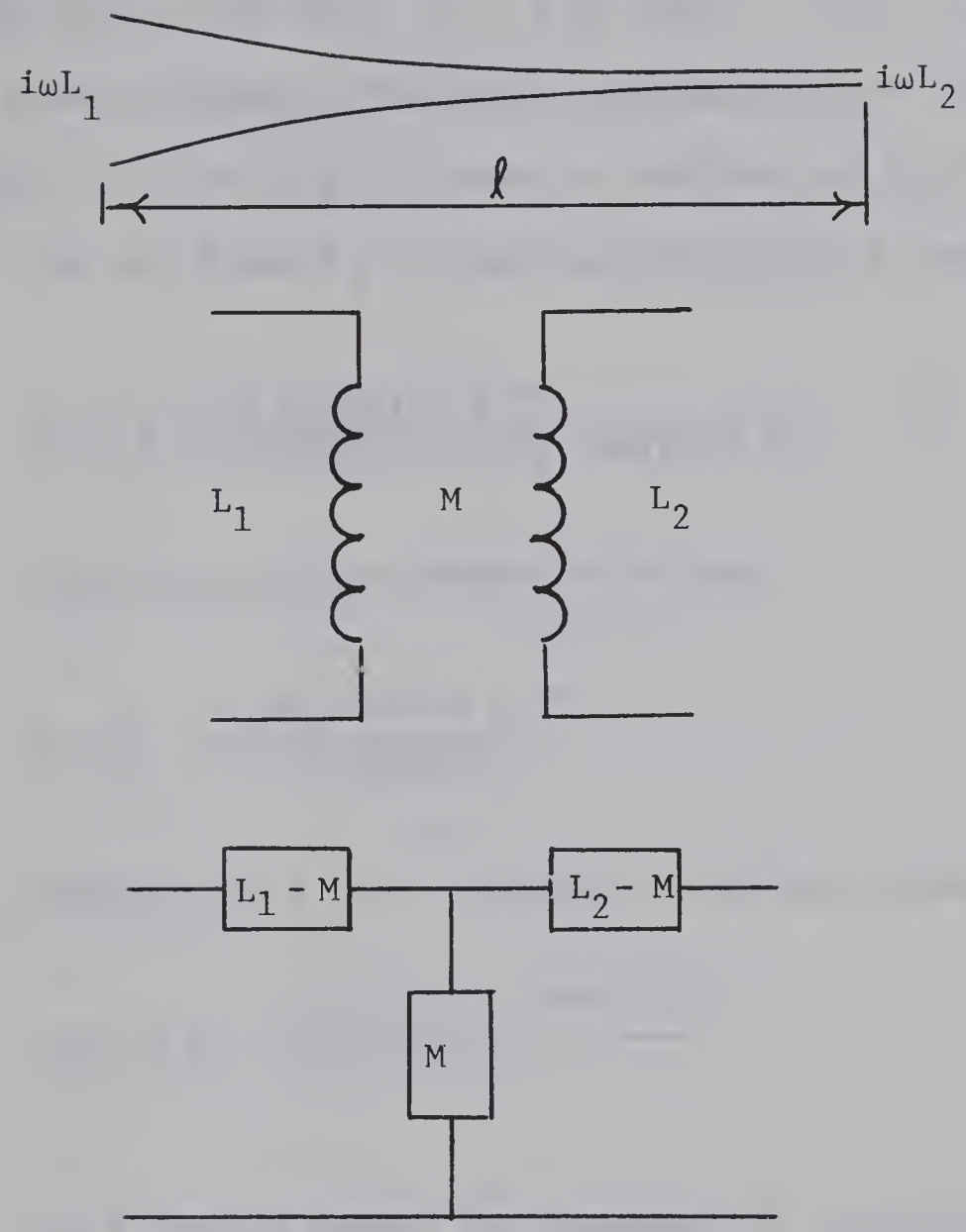

FIGURE 3

Electrical analog of horn

L_1 may be determined by an open circuit on the secondary; or in the case of the horn, $Z_\ell = \infty$ so that $\dot{\xi}_2 = 0$. L_2 may be determined in a similar manner. The mutual impedance $M_{12} = i\omega M$ is the ratio of $p_2 S_2$ to $\dot{\xi}_1$ for rigid closure of the horn at S_2; i.e., $Z_\ell = \infty$.

For $x = 0$ and $Z_\ell = \infty$ the expression for $\dot{\xi}_1$ becomes

$$\dot{\xi}_1 = \frac{i \sin[\beta\ell]\psi \, e^{i\omega t}}{Z_o \, i \sin[\beta\ell] + \rho_o c S_1 \cos[\beta\ell + \theta]}$$

The driving point impedance is then

$$Z = Z_o + \frac{\rho_o c S_1 \cos[\beta\ell + \theta]}{i \sin[\beta\ell]}$$

Subtracting Z_o the impedance of the horn itself is:

$$i\omega L_1 = Z_1 = \frac{i \rho_o c S_1 (\alpha - \beta \cot[\beta\ell])}{k}$$

In a similar manner the impedance at the other end of the horn is:

$$Z_2 = i\omega L_2 = - \frac{i \rho_o c S_2 (\alpha + \beta \cot[\beta\ell])}{k}$$

In finding M the analysis is simpler if $Z_o = 0$. At $x = 0$ with $Z_\ell = \infty$;

$$\dot{\xi}_1 = \frac{i \sin[\beta\ell]\psi \, e^{i\omega t}}{\rho_o c S_1 \cos[\beta\ell + \theta]}$$

Again with $Z_\ell = \infty$ and $Z_o = 0$;

$$p_2 = \frac{e^{-\alpha\ell} \cos[\theta]\psi\ e^{i\omega t}}{S_1 \cos[\beta\ell + \theta]}$$

The force at $x = \ell$ is;

$$S_2 p_2 = \frac{\beta\sqrt{S_2 S_1}\ \psi\ e^{i\omega t}}{k\ S_1 \cos[\beta\ell + \theta]} \qquad \text{since } e^{-\alpha\ell} = \sqrt{\frac{S_1}{S_2}}$$

$$M_{12} = i\ M = \frac{S_2 p_2}{\dot{\xi}_1} = -\frac{i\ \rho_o c\ \beta\sqrt{S_1 S_2}}{k \sin[\beta\ell]}$$

If the horn is driven by a piston of negligible impedance then the driving point impedance of a loaded horn is from the equivalent T network;

$$Z = \frac{Z_1 Z_2 - M_{12}^2 + Z_1 Z_\ell}{Z_2 + Z_\ell}$$

Z_ℓ = load impedance

$Z_\ell = \rho_o c S_2 (R + iX)$

R and X are frequency dependent quantities which are dimensionless. They will be discussed later in this chapter.

To investigate the velocity transforming effects of the horn we have from the equivalent network;

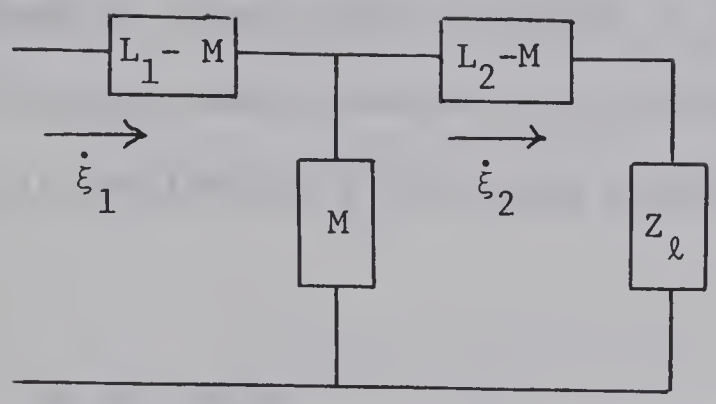

$$(\dot{\xi}_1 - \dot{\xi}_2)M_{12} = \dot{\xi}_2(Z_2 + Z_\ell)$$

$$\frac{\dot{\xi}_2}{\dot{\xi}_1} = \frac{M_{12}}{Z_2 + Z_\ell}$$

$$\frac{\dot{\xi}_2}{\dot{\xi}_1} = -\frac{i\cos[\theta]\sqrt{S_1 S_2}}{S_2\{R\sin[\beta\ell] + i<X\sin[\beta\ell] - (\sin[\theta]\sin[\beta\ell] + \cos[\theta]\cos[\beta\ell])>\}}$$

When $\beta\ell = \pi n$ where n is an integer the velocity transformation reduces to:

$$\frac{\dot{\xi}_2}{\dot{\xi}_1} = \pm\sqrt{\frac{S_1}{S_2}}$$

This last relationship illustrates that the effect of the horn when in resonance is to increase the velocity and pressure by the ratio of the root of the end areas.

3.2 Directivity

In order to calculate the pressure distribution at a distance

away from the radiating end of the horn it is convenient to consider the horn made up of many point sources. A small element of area $d\underline{S}$ of a vibrating source mounted in an infinite baffle so that the radiation is confined to a half space produces a pressure dp given by [12]:

$$dp = \frac{i\rho_o ck\ \underline{U}.d\underline{S}\ e^{i(\omega t - kr')}}{2\pi r'} \qquad \text{(see Appendix H)}$$

$\underline{U}e^{i\omega t}$ = velocity of the element $d\underline{S}$

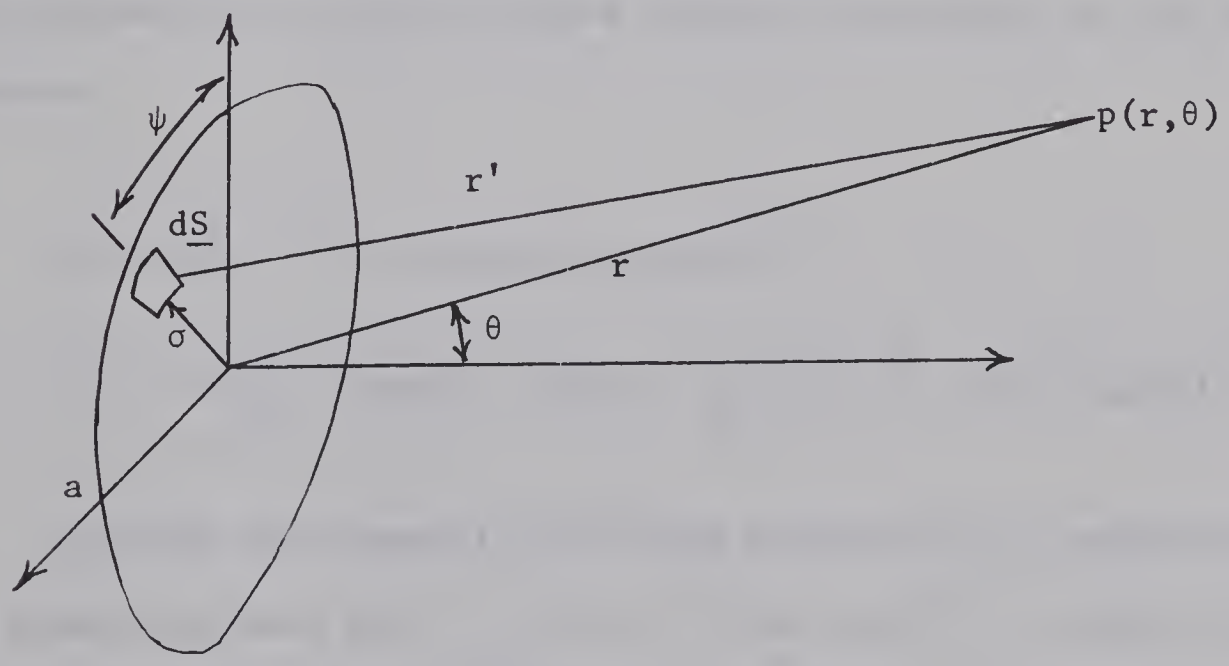

FIGURE 4

Diagram to obtain directivity function

In order to find the pressure at a point in the half space it is necessary to integrate over the source area. The baffle is assumed to be rigid so that everywhere on the baffle $\underline{U}.d\underline{S} = 0$.

$$p(r,\theta) = \iint \frac{i\rho_o ck\ \underline{U}.d\underline{S} e^{i(\omega t - kr')}}{2\pi r'}$$

In the case of the horn the velocity $\underline{U} = \dot{\xi}_2$ and is everywhere normal to $\underline{S}$.

If p is to be evaluated at positions which are far enough from the source then r' may be replaced by r in the denominator of the expression for $p(r,\theta)$. The r' which appears in the exponent may not be replaced by r since this term accounts for the relative phase differences due to radiation from different positions on the vibrating surface.

$$r' = \{r^2 + \sigma^2 - 2r\sigma\sin[\theta]\ \cos[\psi]\}^{1/2}$$

$$r' = r + \frac{\sigma^2}{2r} - \sigma\sin[\theta]\ \cos[\psi] - \frac{r}{8}\{\frac{\sigma^2}{r^2} - \frac{2\sigma}{r}\sin[\theta]\ \cos[\psi]\}^2 + \ldots$$

In order that terms in the above expression not contribute to the phase they must be $<< \lambda$. If $r >> \sigma$ so that $\frac{\sigma^2}{r} << \lambda$ then r' may be approximated in the exponent as;

$$r' = r - \sigma\sin[\theta]\ \cos\ [\psi]$$

hence

$$p = \left[\frac{i\,\rho_o ck}{2\pi r}\, U\, e^{i(\omega t)}\right]\left[\int_o^a \sigma\, d\,\sigma \int_0^{2\pi} e^{ik\,\sigma \sin[\theta]\,\cos[\psi]}\, d\psi\right]$$

This expression is integrated to obtain:

$$p = \frac{i\,\rho_o cka^2}{2r}\, Ue^{i(\omega t - kr)}\, \frac{2\,J_1(ka\,\sin[\theta])}{ka\,\sin[\theta]}$$

From this expression we expect the phase of the wave transmitted from the horn to be that of a spherical wave, i.e., e^{-ikr}.

The amplitude is proportional to r as in a sperical wave but there is an additional dependence upon the azimuthal angle. The directivity term $\frac{2\,J_1(ka\,\sin[\theta])}{ka\,\sin[\theta]}$ is seen to be dependent upon the radius of the radiating aperture and upon the azimuthal angle θ.

3.3 Load impedance

The term Z_ℓ, or the load impedance, has already been used in previous sections of this thesis. This term is now discussed in detail, following closely reference [13].

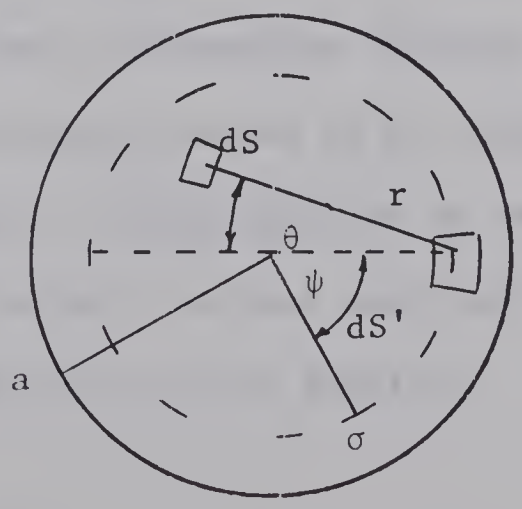

FIGURE 5

Diagram to obtain reaction force on a vibrating piston

Each element of a vibrating piston in an infinite baffle produces a pressure wave which creates a force on the rest of the piston. A small element dS produces a pressure adjacent to an element dS' given by [12].

$$dp = \frac{i\,\rho_o ck}{2\pi r}\, U\, e^{i(\omega t - kr)} dS$$

$Ue^{i\omega t}$ = velocity of the vibrating piston and is normal to dS.

For the horn $Ue^{i\omega t} = \dot{\xi}_2$.

The total pressure adjacent to the element dS' is;

$$p = \iint \frac{i\,\rho_o ck}{2\pi r}\, U\, e^{i(\omega t - kr)} dS$$

The total reaction force on the piston is then;

$$\underline{f_r} = -\iint p\, d\underline{S}'$$

The minus sign occurs because for positive pressures the force is into the piston.

Realizing that the pressure adjacent to dS' caused by dS is the same as the pressure caused by dS' adjacent to dS makes the integration easier. The integration is carried out only over the inner circle of radius σ so that each pair of elements are considered only once. The result is then doubled.

$$dS = r\, d\theta\, dr$$

The maximum length in the direction θ is $2\sigma\cos[\theta]$ so that r is integrated from 0 to $2\sigma\cos[\theta]$. The limits on θ are $-\frac{\pi}{2}$ to $\frac{\pi}{2}$.

$$dS' = \sigma d\sigma d\psi$$

The limits on ψ are 0 and 2π while the limits on σ are 0 to a.

$$\underline{f_r} = -\frac{i\,\rho_o ck}{\pi}\,\underline{U}\,e^{i\omega t}\int_o^a \sigma d\sigma \int_0^{2\pi} d\psi \int_{-\pi/2}^{\pi/2} d\theta \int_0^{2\sigma\cos[\theta]} e^{-ikr}\,dr$$

$$\int_{-\pi/2}^{\pi/2} d\theta \int_0^{2\sigma\cos[\theta]} e^{-ikr}\,dr = \frac{\pi}{ik} + \frac{2i}{k}\int_0^{\pi/2} e^{-i2k\sigma\cos[\theta]}\,d\theta$$

$$\int_0^{\pi/2} e^{-i2k\sigma\cos[\theta]}\,d\theta = \frac{\pi}{2}\left\{1 - \frac{1}{2^2}(2k\sigma)^2 + \frac{1.3(2k\sigma)^4}{2.4.4!} \ldots\right\}$$

$$-i\left\{2k\sigma - \frac{2}{3.3!}(2k\sigma)^3 \ldots\right\}$$

The above integral has been evaluated by expanding the exponential term and using;

$$\int_0^{\pi/2} \cos^n[x]\,dx = \frac{1.3\ldots(n-1)}{2.4\ldots n}\,\frac{\pi}{2} \qquad n \text{ even}$$

$$\int_0^{\pi/2} \cos^n[x]\,dx = \frac{2.4\ldots(n-1)}{1.3\ldots n} \qquad n \text{ odd, and greater than 1}$$

After executing the remaining integrations one obtains:

$$\underline{f_r} = -\rho_o c\pi a^2 \, \underline{U} \, e^{i\omega t}[R(2ka) + iX(2ka)]$$

where $$R(x) = \frac{x^2}{2.4} - \frac{x^4}{2.4^2.6} + \frac{x^6}{2.4^2.6^2.8} \quad \ldots$$

$$X(x) = \frac{4}{\pi}\left\{\frac{x}{3} - \frac{x^3}{3.5} + \frac{x^5}{3^2.5^2.7} \quad \ldots\right\}$$

Hence

$$Z_r = \rho_o c\pi a^2[R(2ka) + iX(2ka)]$$

For the horn $\pi a^2 = S_2$ so that

$$Z_\ell = Z_r = \rho_o c S_2[R(2ka) + iX(2ka)]$$

3.4 Design of horn

The parameters of the exponential horn are frequency dependent so that as a starting point in designing a horn the operating frequency was first specified. One megahertz was chosen for the following reasons:

[1] The wave length of one megahertz acoustic waves in water is 1.48 mm. Examination of the directivity function

reveals that the smaller the aperture relative to the wave length the more widely scattered is the radiation. A wave length of 1.48 mm. meant that it was possible to machine a mandrel having a smaller radius of the order of a wave length.

[2] One megahertz thickness-mode barium titanate piezoelectric discs were commercially available. The diameter of these discs was one centimeter.

[3] Electrical circuitry which functions at one megahertz would be relatively easy to build.

The larger diameter of the horn was chosen to be 1.5 cm. in order to facilitate mounting of the 1 cm. crystal.

In designing the smaller end of the horn three factors had to be considered.

[1] Directivity function

[2] Radiation impedance; $R(x) + iX(x)$

[3] Ease of machining a mandrel having a sufficiently small radius at the smaller end.

By choosing the smaller diameter of the horn to be 1.5 mm. (approximately one wave length at one megahertz) the directivity criterion would be satisfied. At an azimuthal angle of 15 degrees the amplitude is 96 percent of the on axis amplitude. The values for $R(x)$ and $X(x)$ are 1 and .2 respectively so that an appreciable amount of the power that is incident on the apperture is transmitted.

If the radius of the aperture becomes much less than λ then the terms R(x) and X(x) approach 0. For small apertures ($r << \lambda$) high acoustic fields are necessary to produce adequate radiated power. Since high fields cause degassing and cavitation they are undesirable. Even for the radius used occasionally bubbles appeared in the narrow neck of the horn indicating degassing. An air bubble in the end of the horn greatly deteriorates the horn performance as is illustrated in chapter 4.

Only the flare constant "m" remains to be specified. Factors affected by this parameter are the cut-off frequency and the phase angle between pressure and velocity. The terms u_1 and u_2 which appear in the expression for the velocity potential become entirely real for certain values of m.

$$u_1 = -\alpha + i\beta$$

$$u_2 = -\alpha - i\beta$$

$$\beta = \frac{i}{2}\sqrt{4k^2 - m^2}$$

Hence the waves become evanescent for $m = 2k = \frac{4\pi}{\lambda}$.

The cut-off frequency is defined as the frequency for which $m = 2k$.

A value of $-.848\ cm^{-1}$ was chosen for m so that the cut-off frequency is specified as 10 k hertz. For a tuned horn ($\beta\ell = n\pi$;

n is integer) the phase angle between pressure and velocity is given by θ.

$$\theta = \tan^{-1} \frac{\alpha}{\beta}$$

θ < 1 degree

The small value of θ results in a power factor very close to one.

CHAPTER 4

EXPERIMENTAL

4.1 Tank construction

Mounting details for the transmitting horn and detector are presented in figure [6]. The water tank which measured 2 x 1 x 1 meters was constructed of 3/4 inch plywood. The size of the tank was larger than the scanning apparatus required. The large tank size resulted in a path difference between signals reflected from the walls of the tank and the signals of interest. Because the experiments were run on a pulsed basis the path difference resulted in isolation of reflected signals from signals of interest. The horn was mounted in the center of one of the ends of the tank so that the small aperture would be in an infinite baffle and so that the back of the piezoelectric disc would not be mass loaded by water.

In order to reduce any electrical pick up through the water the side of the crystal facing the water was grounded.

Another piezoelectric disc was mounted so that it would rotate about the aperture of the horn. A linear potentiometer was mechanically fastened to the rotating arm so that it was possible to obtain an electrical signal proportional to the azimuthal angle e which indicates the position of the plane mounted disc relative to the horn aperture.

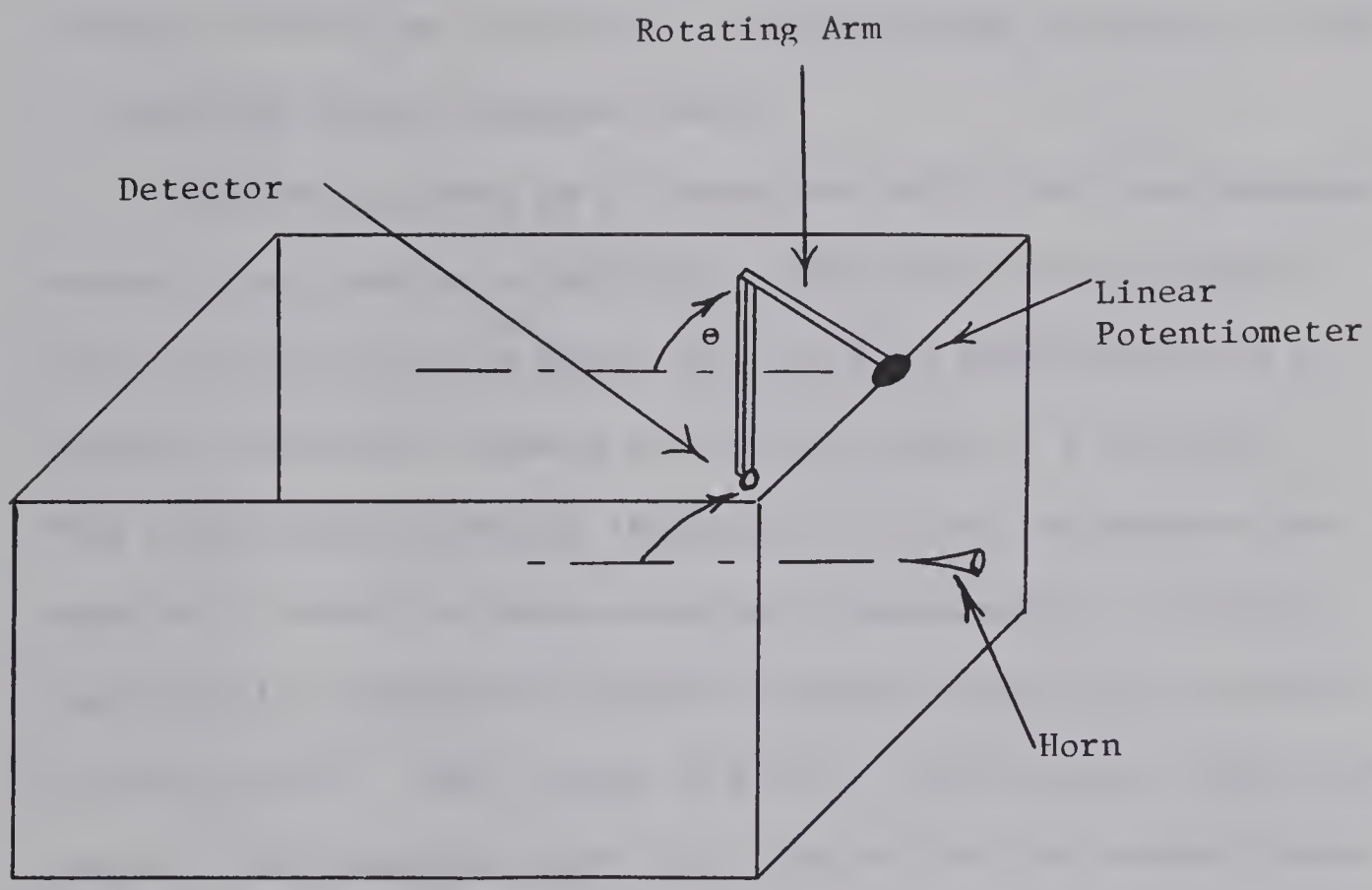

FIGURE 6

Tank geometry

The rotating arm is such that the detector rotates about the horn aperture in a plane parallel to the bottom of the tank. The horn axis lies in the plane of rotation of the disc.

4.2 Radiation pattern for single horn

4.2.1 Amplitude versus azimuthal angle

In this section experimental measurement of the directivity function of the horn device is described. The effects of various mounting factors on directivity are illustrated by means of plots of amplitude versus azimuthal angle.

The horn was used as a transmitter while the plane mounted crystal functioned as a receiver. Electrical driving signals were one megacycle sine waves of forty volt amplitude while the received electrical signals were on the order of a millivolt. This meant that electrical isolation of 100 db. or greater was required in order to obtain meaningful measurements. Pulsing the acoustic transmitter provided adequate electrical isolation of the receiver. Wave trains of about .1 milliseconds (100 cycles) spaced .9 milliseconds apart were used so that the acoustic wave train reached the receiver in the absence of stray electrical driving signals (the ratio of stray electrical signals from the transmitter to noise from receiver was < 1). Another positive effect of making measurements on a pulsed basis was that acoustic wall reflections and standing waves in the tank were minimized.

Received signals were amplified by a low noise amplifier which was specially designed to work at megacycle frequencies. Further processing involved a circuit which measured the amplitude of the wave trains and held this value until the next

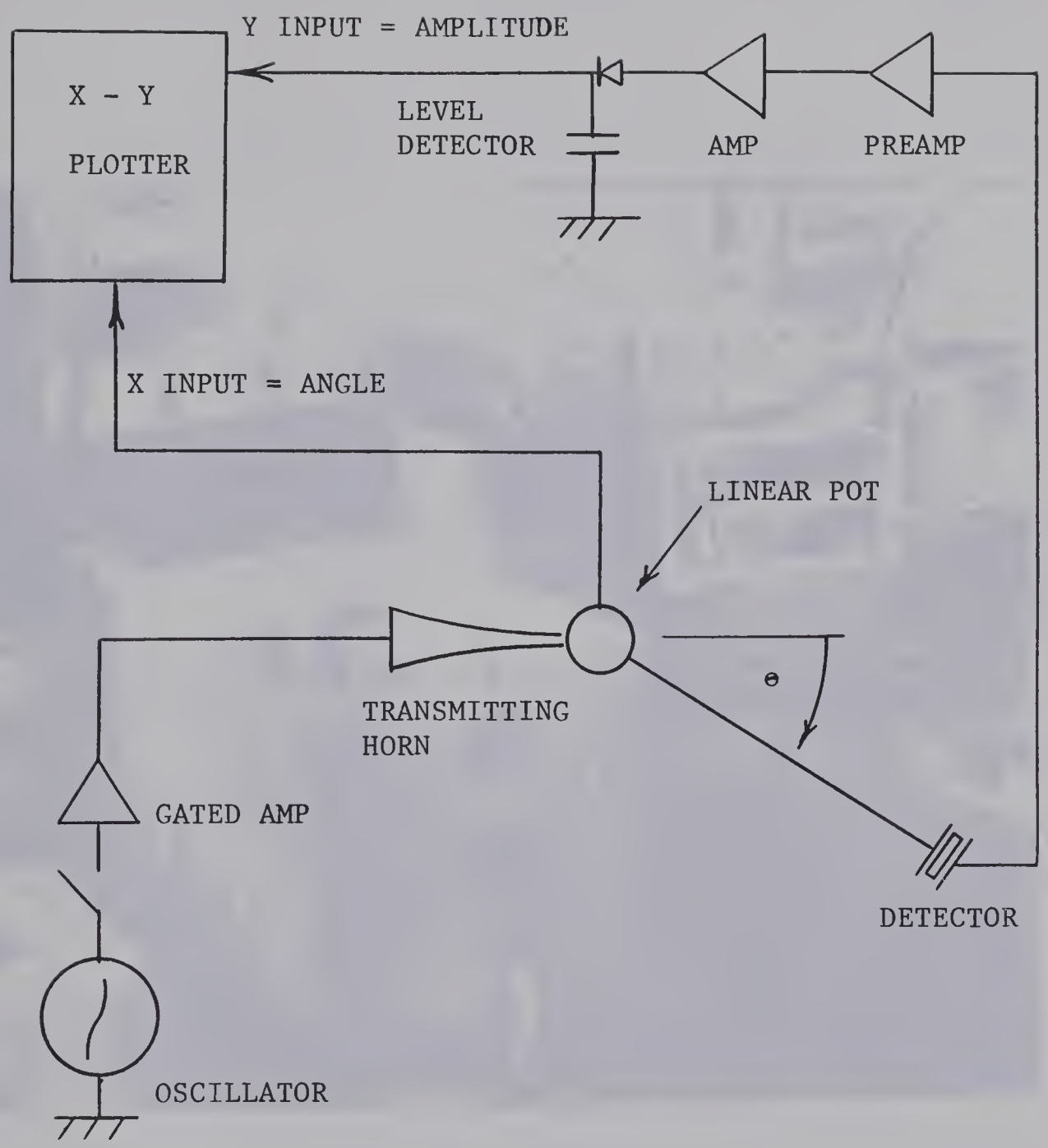

FIGURE 7

Schematic of experimental set up for measuring directivity function

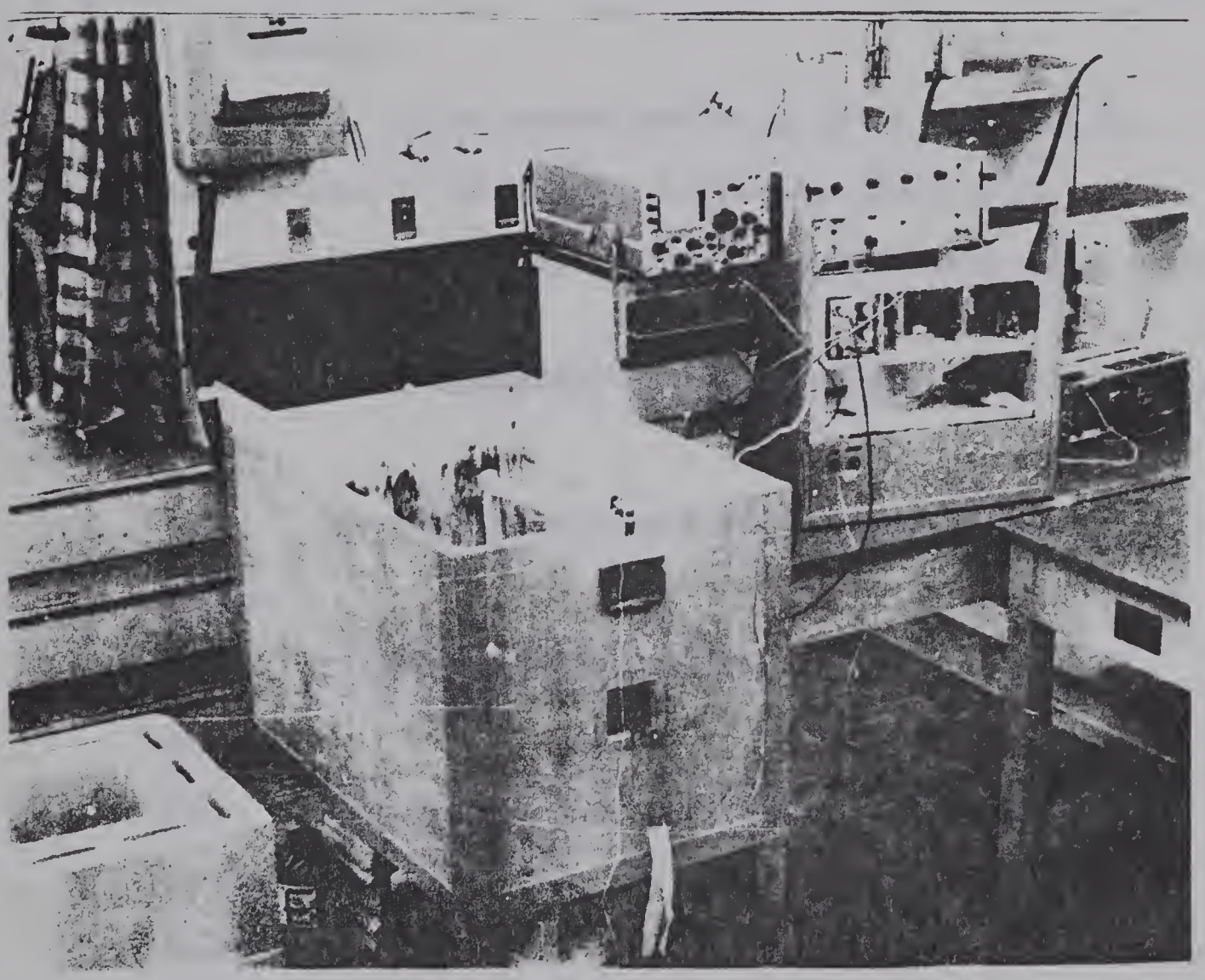

FIGURE 8

Photograph of experimental equipment

wave train was presented to it.

A circuit diagram of the gated oscillator amplifier which provided the driving electrical signals appears in appendix C. The low noise preamplifier and amplitude detector schematics also appear in appendix C.

In section 3.2 the theoretical directivity function for a vibrating piston in an infinite baffle was shown to be $2\,\frac{J_1\,(k\ a\ \sin[\theta])}{k\ a\ \sin[\theta]}$. Experimental mounting conditions which produced results most closely approximating the theoretical predictions are listed below.

[1] The horn aperture was mounted tightly in the baffle.

[2] The wall thickness of the horn was as thin as possible.

[3] The piezoelectric disc was mounted perpendicular to the axis of the horn.

Profiles obtained under the conditions mentioned above were more directional than the theory predicted. This is illustrated in figure [10]. Such an effect is equivalent to a larger effective radiating apperture. In order to develop a theory which would predict accurately the directivity function of the horn a computer program was set up which would assign a fraction of the power

radiated to the copper walls of the horn and the remainder to the water filled aperture.

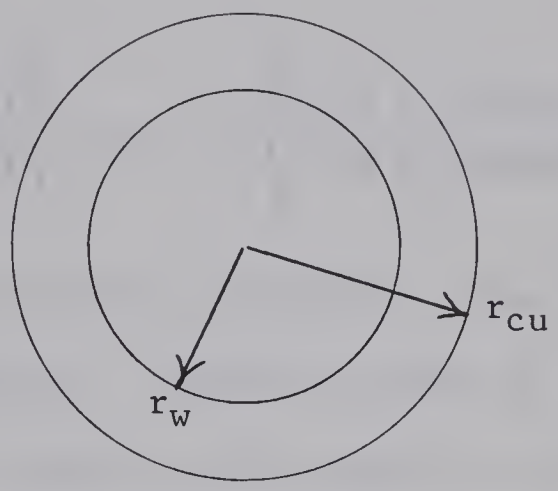

FIGURE 9

Radiating aperture

The amplitude of vibration within the water filled area is normalized to 1 while the amplitude of vibration in the copper area is assumed to be some fraction "f" of that of the center area. Assuming linear superposition the amplitude at a large distance from the horn is proportional to $\frac{J_1 (k\, r_w \sin[\theta])}{k\, r_w \sin[\theta]}$

for the center area and is proportional to

$$f \times \left\{ \frac{J_1(k\, r_{cu} \sin[\theta])}{k\, r_{cu} \sin[\theta]} - \frac{J_1(k\, r_w \sin[\theta]}{k\, r_w \sin[\theta]} \right\}$$

for the ring shaped copper area. The total directivity function is proportional to:

$$f \left\{ \frac{J_1(k\, r_{cu} \sin[\theta])}{k\, r_{cu} \sin[\theta]} \right\} + (1 - f) \left\{ \frac{J_1(k\, r_w \sin[\theta]}{k\, r_w \sin[\theta]} \right\}$$

The APL program presented in Appendix D was written to evaluate the above equation. Different values of f were used and then the calculated results were compared to the experimental results. Closest correlation occurred for f = 1. Hence for calculations the directivity function $\frac{2\, J_1(k\, a \sin[\theta])}{k\, a \sin[\theta]}$ where a is the outer diameter of the horn should be used.

The preceding results strongly suggest that the metal horn itself vibrates. This result is not surprising when one considers the lack of rigidity of the thin electroplated structure.

At this point it should be noted that the directivity function above assumes that the velocity of the water aperture is in phase with the velocity of the copper. The agreement between experiment and calculations using f = 1 suggests that acoustic coupling to the horn shell is not a consequence of the 0 ring. If the 0 ring were the driving mechanism then the vibrating copper at the aperture would be out of phase with the vibrations in the aperture since the velocity of sound in copper is much different than in water.

By the theorem of reciprocity [14] the horn should display the same directional characteristics when used as a receiver or as a transmitter. Experimentally this was found to be the case. The plane mounted disc was used as the transmitter and rotated about the horn which was used as a receiver. In this manner plane waves were presented to the horn aperture over a range of azimuthal angle of $\pm$ 30 degrees. Normalized plots of amplitude versus azimuthal angle were the same for both transmitter and receiver. This result again indicates that the larger effective aperture is due to vibration of the copper walls. Another result worthy of note is that the directionality does not increase with stronger acoustic fields but is constant over a wide range of intensities.

Various different mounting conditions that were tried are illustrated graphically in figures [12] thru [16]. Since the metal of the horn was thought to be vibrating it was possible that by contouring the end of the horn less directivity could be obtained. However the best results were obtained by simply making the walls of the horn as thin as possible.

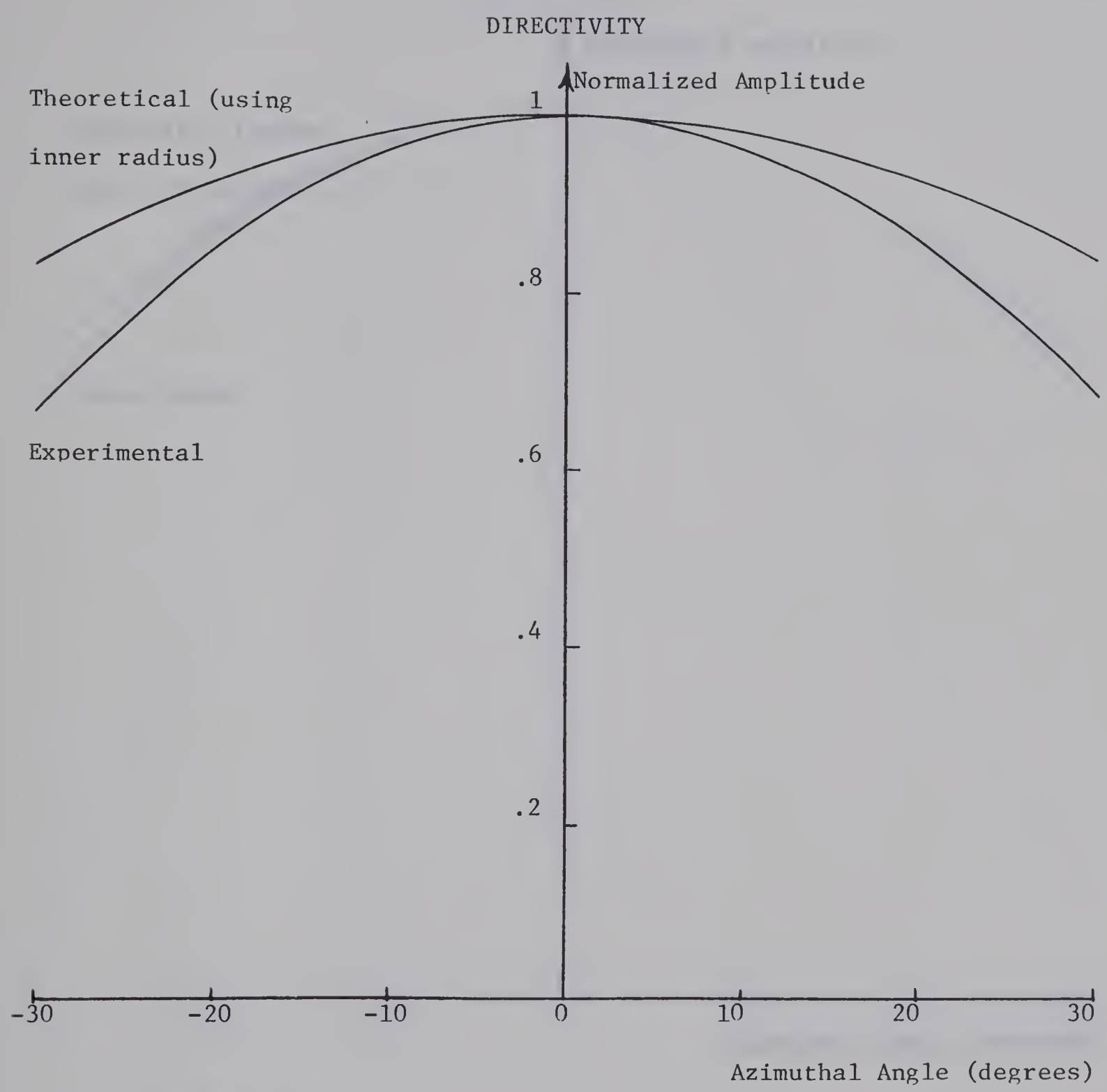

FIGURE 10

Comparison of theoretical and calculated directivity for horn aperture of inner radius .1 cm. and outer radius of .15 cm.

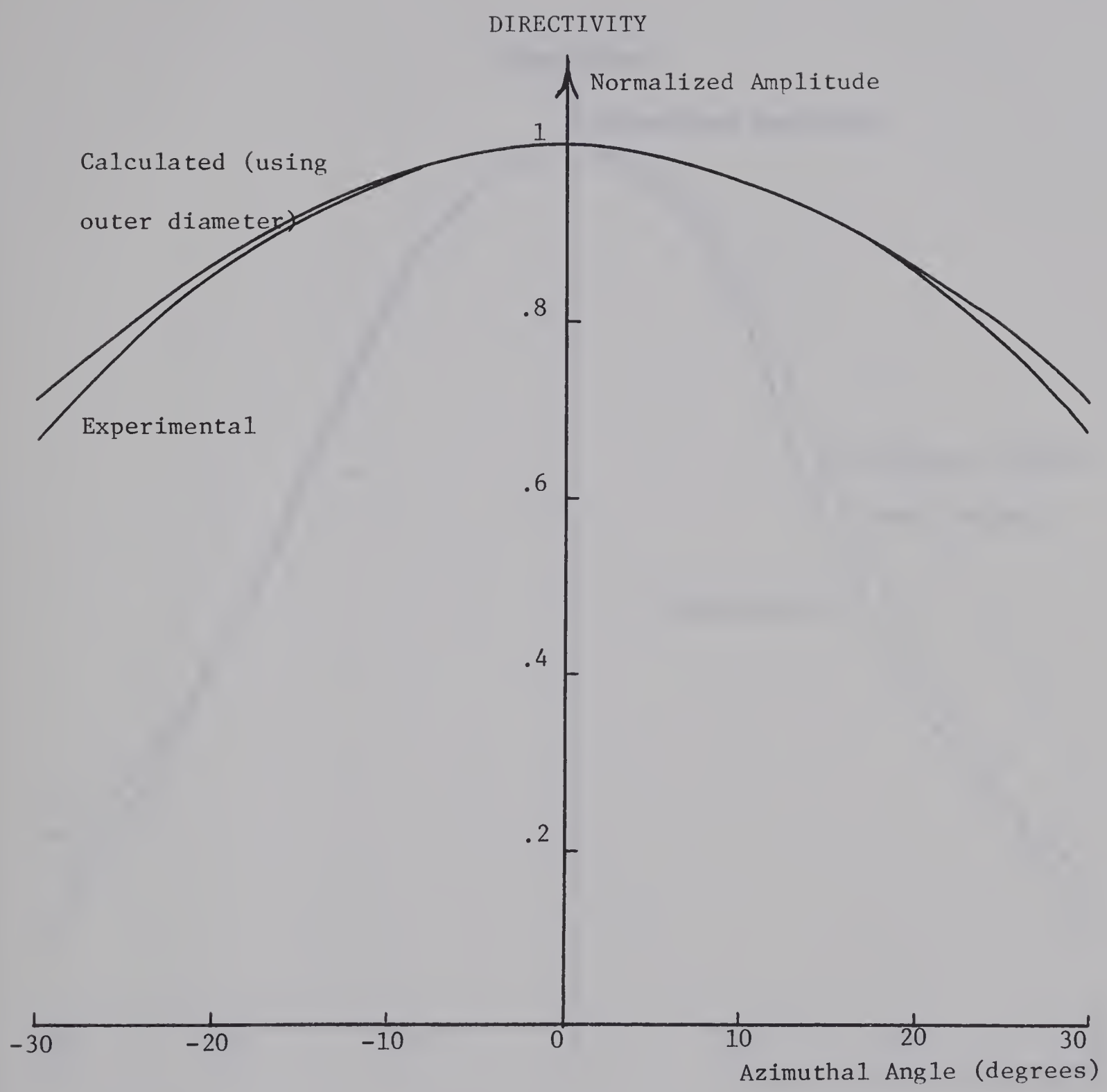

FIGURE 11

Comparison of experimental data with modified theory which takes into account vibrating copper. (For modified theory see pages 29 - 31.)

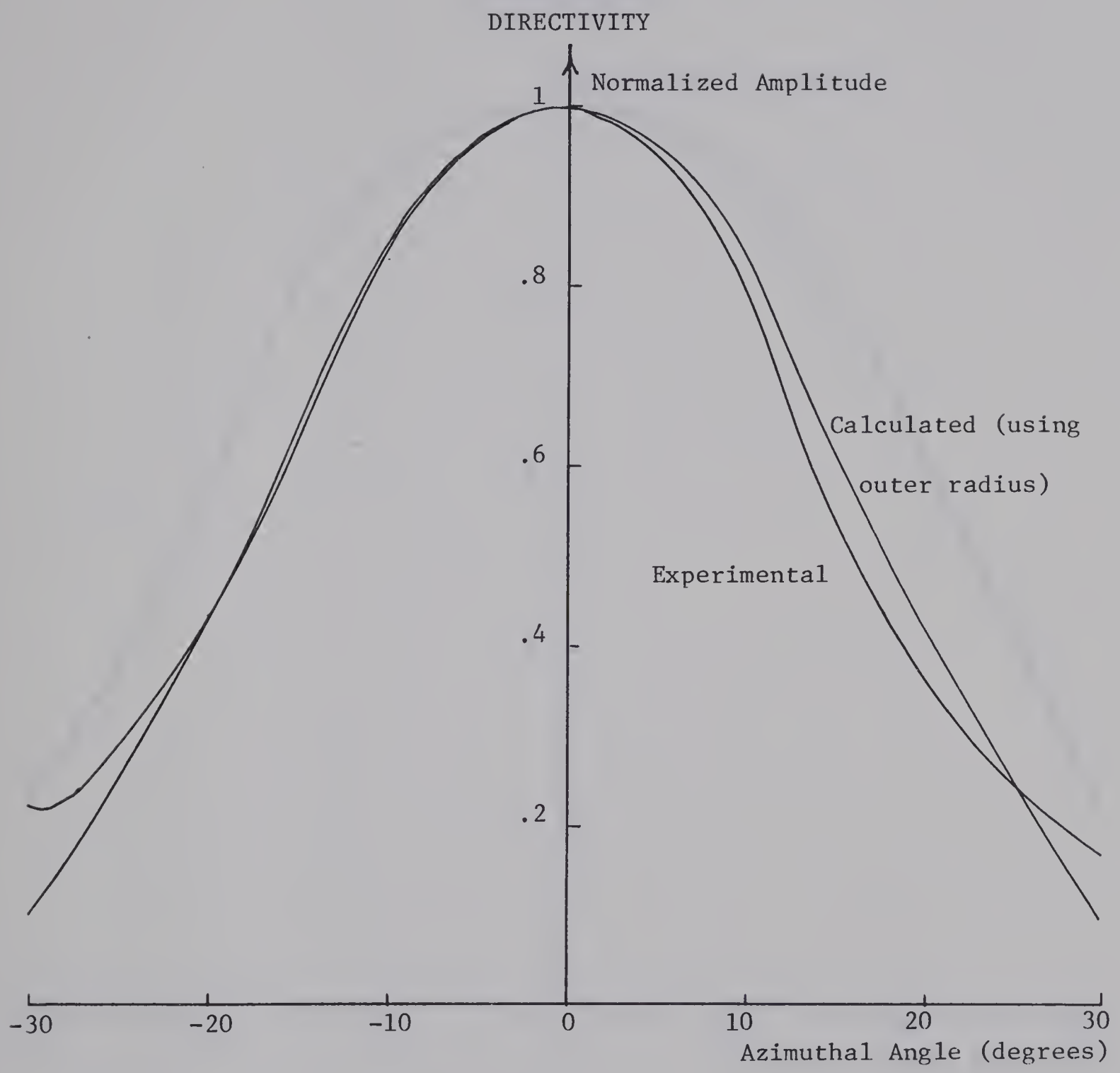

FIGURE 12

Directivity for thick walled horn

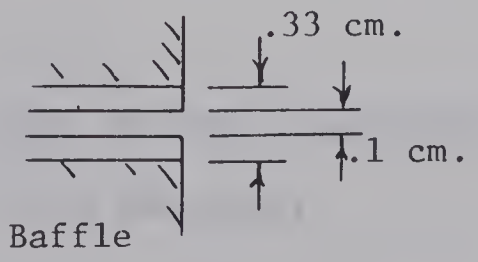

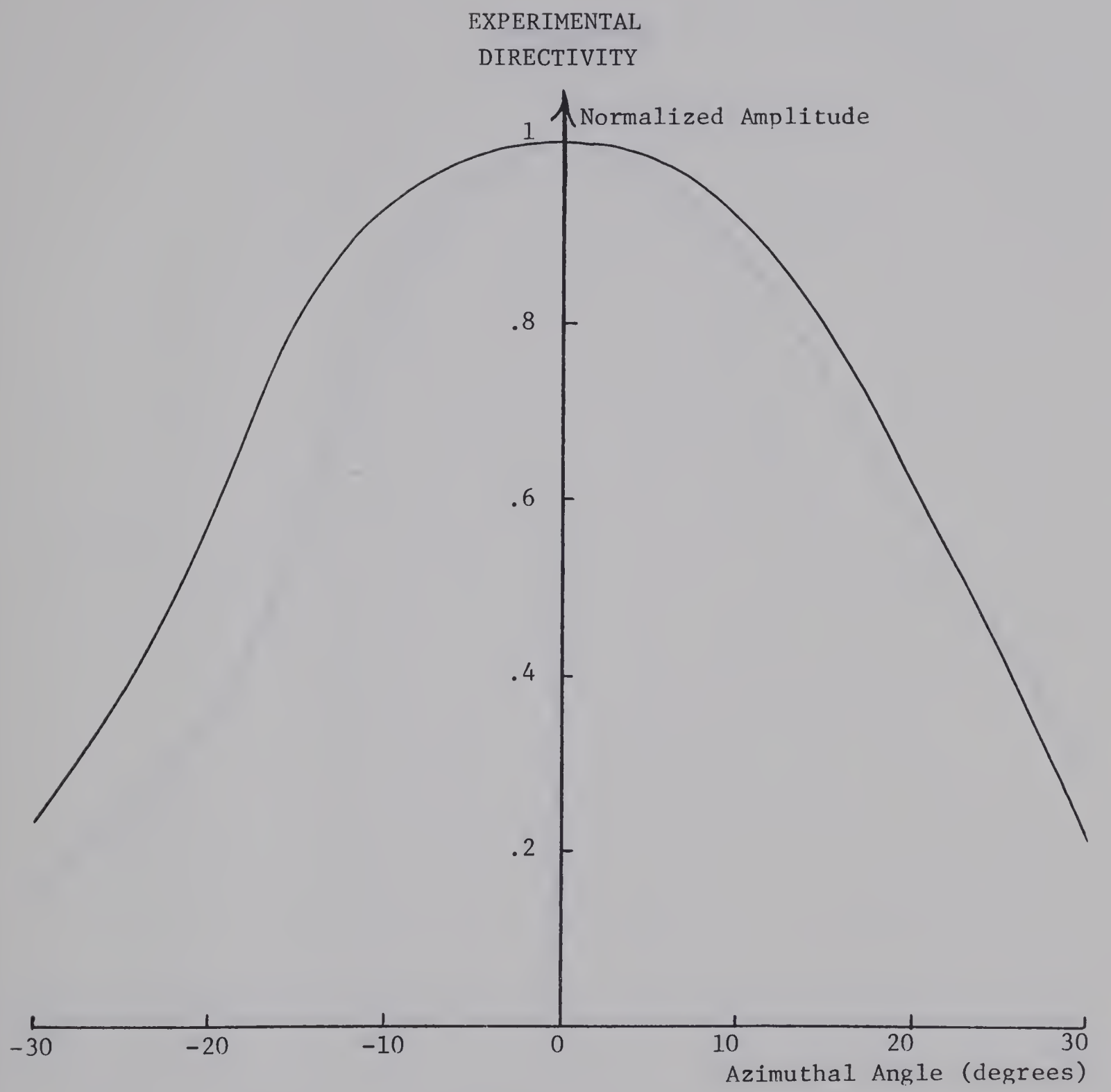

FIGURE 13

Directivity for concave horn end

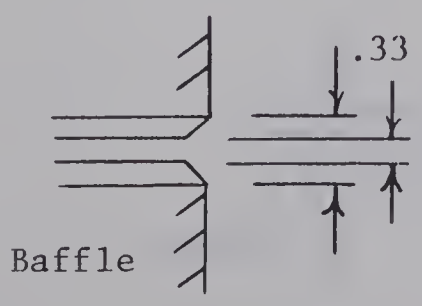

End of horn countersunk

with #46 drill

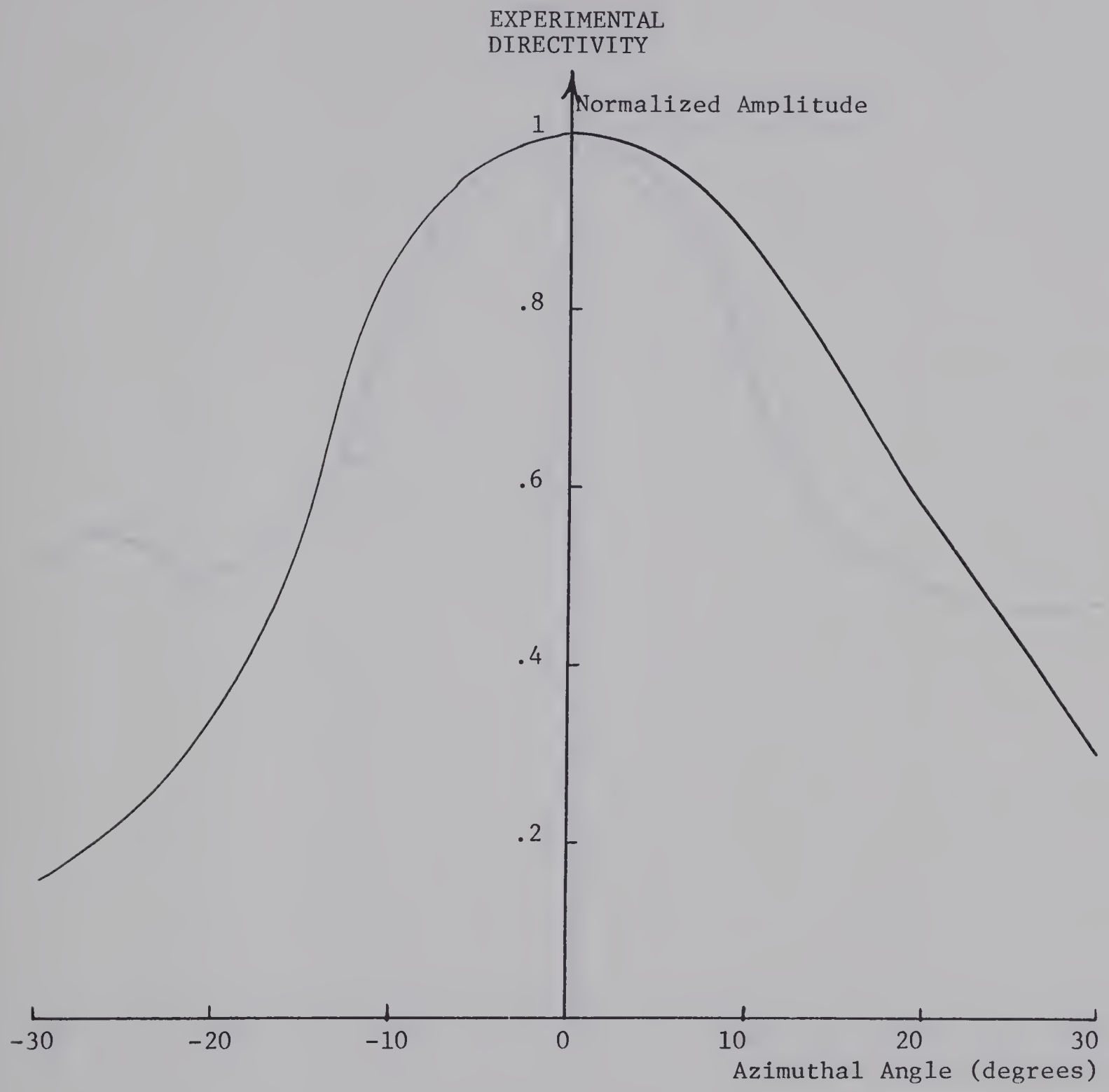

FIGURE 14

Directivity for horn with concave end protruding from baffle

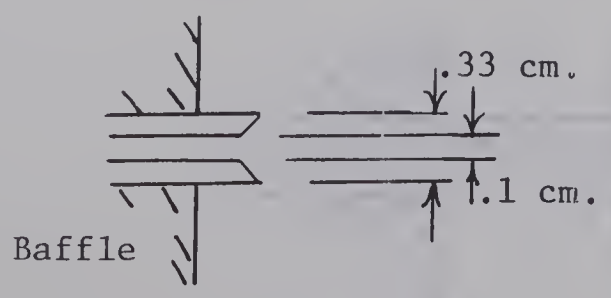

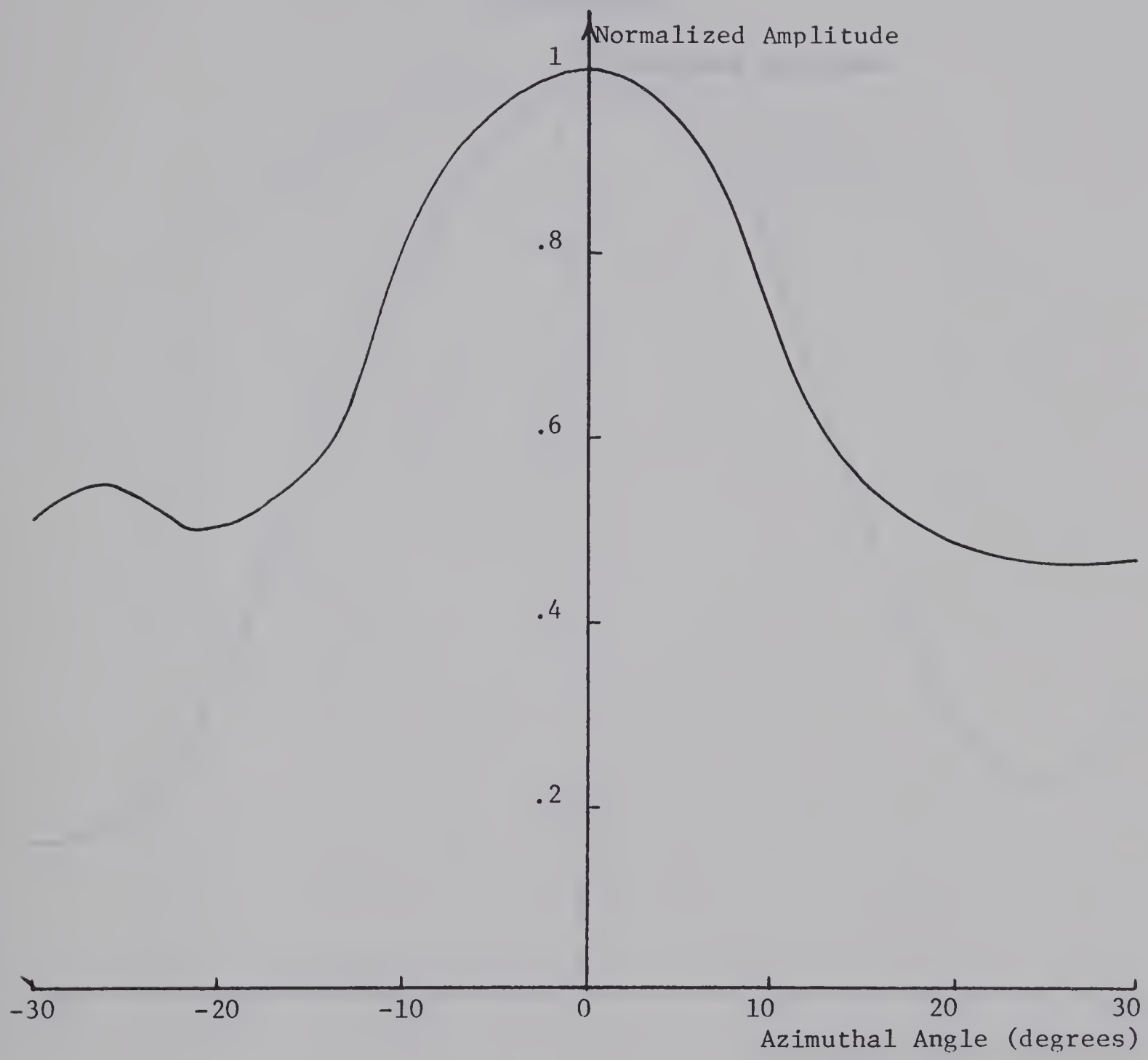

FIGURE 15

Directivity of horn with convex end

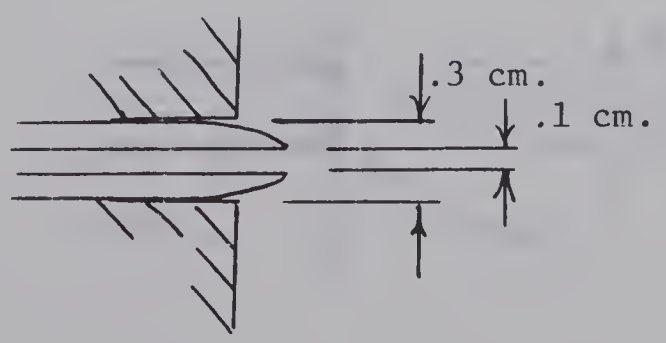

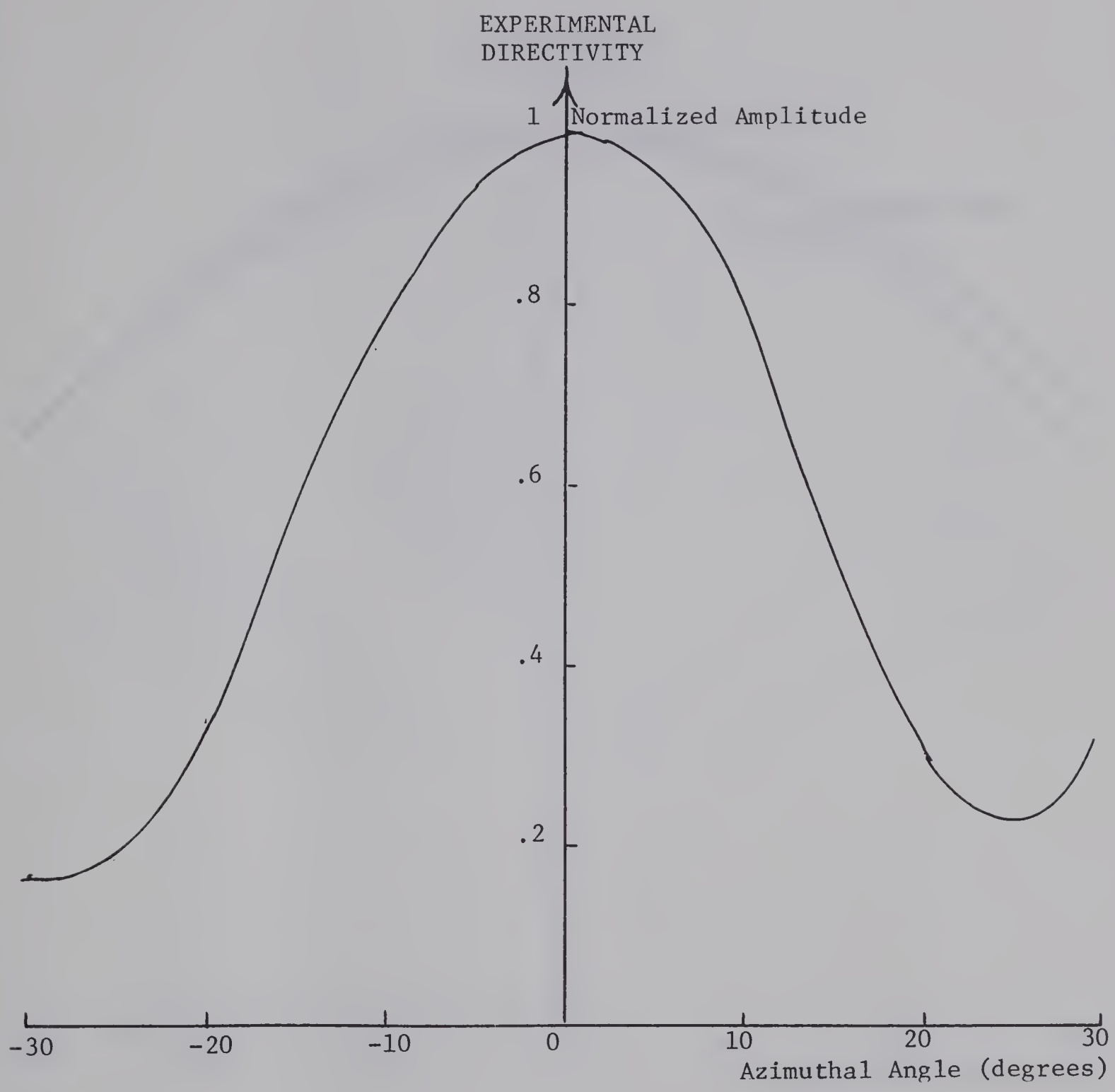

FIGURE 16

Convex horn end, baffle aperture filled with wood putty

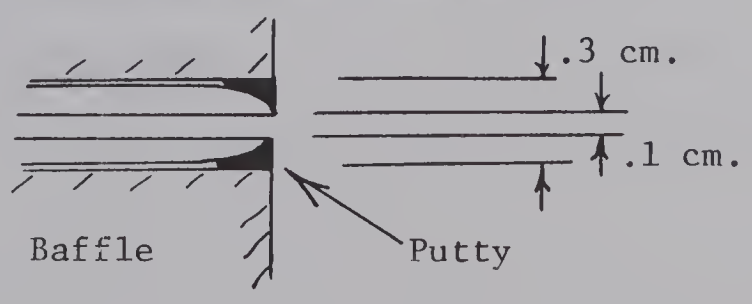

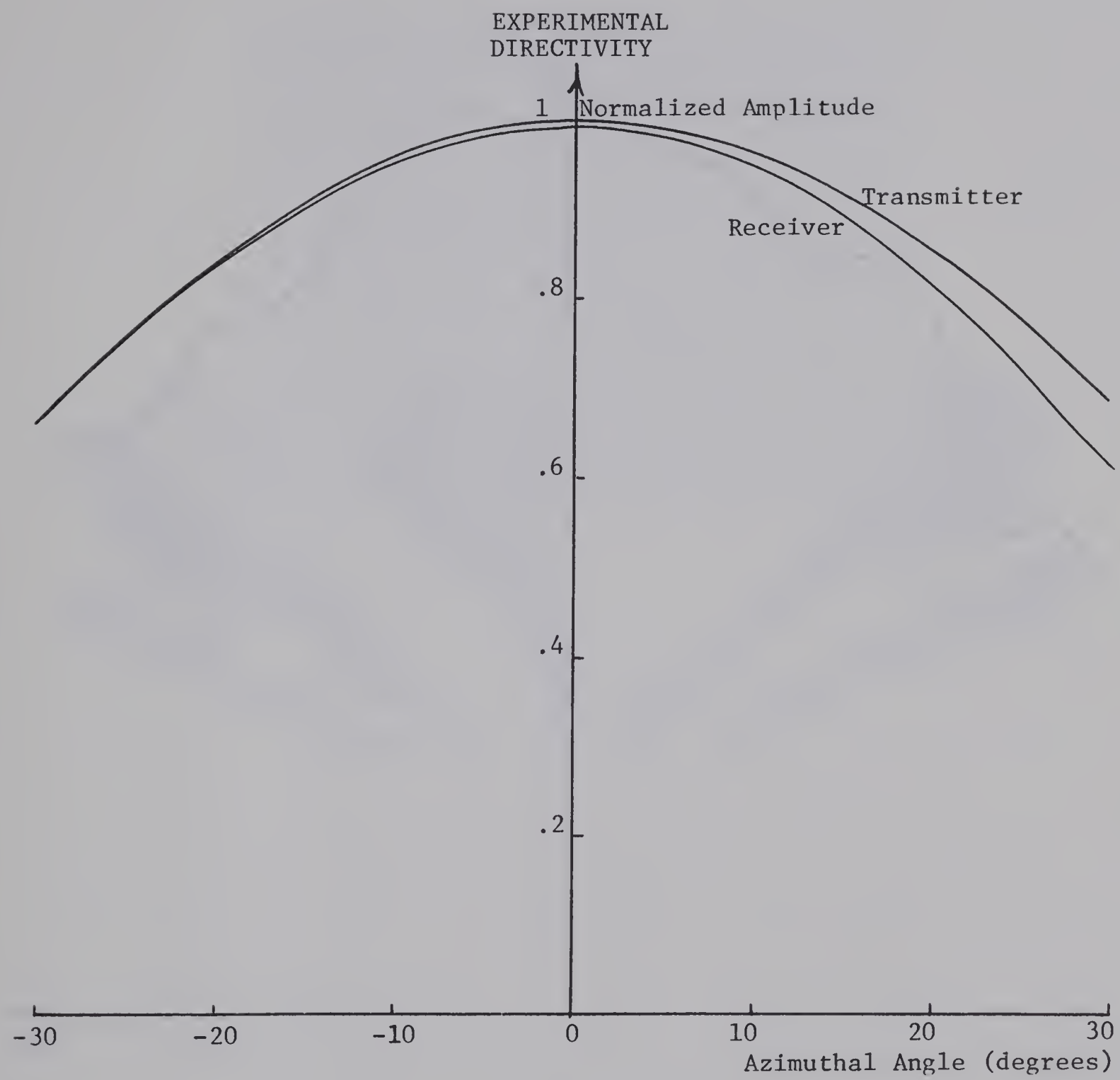

FIGURE 17

Comparison of directivity plots for horn used as a transmitter and as a receiver

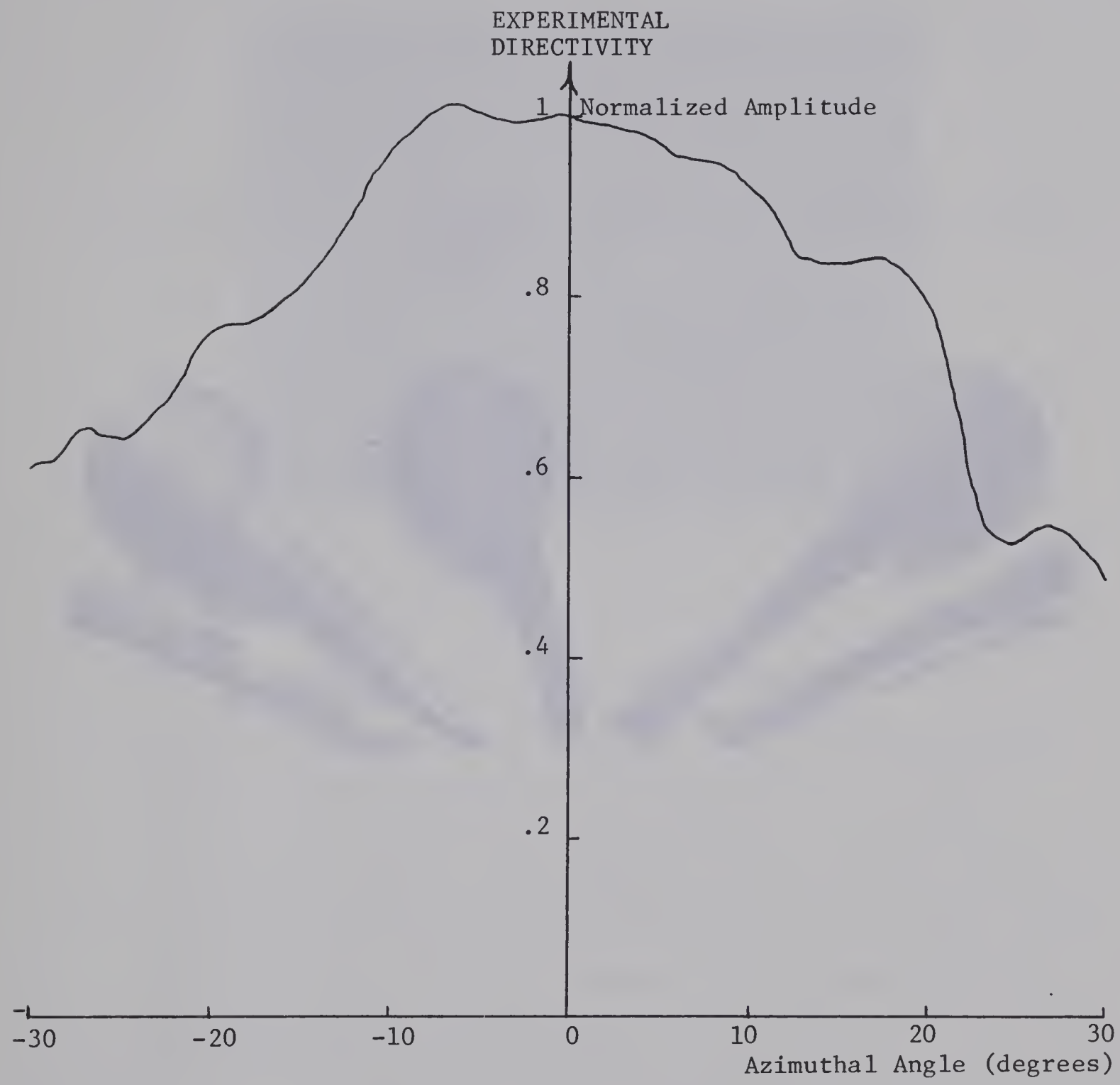

FIGURE 18

Directivity for horn with air bubble in aperture.

Due to normalization the plot does not show the greatly reduced signal level. Signal levels were so small that electrical noise prevented obtaining a reasonable plot.

FIGURE 19

Photograph of various radiating apertures.

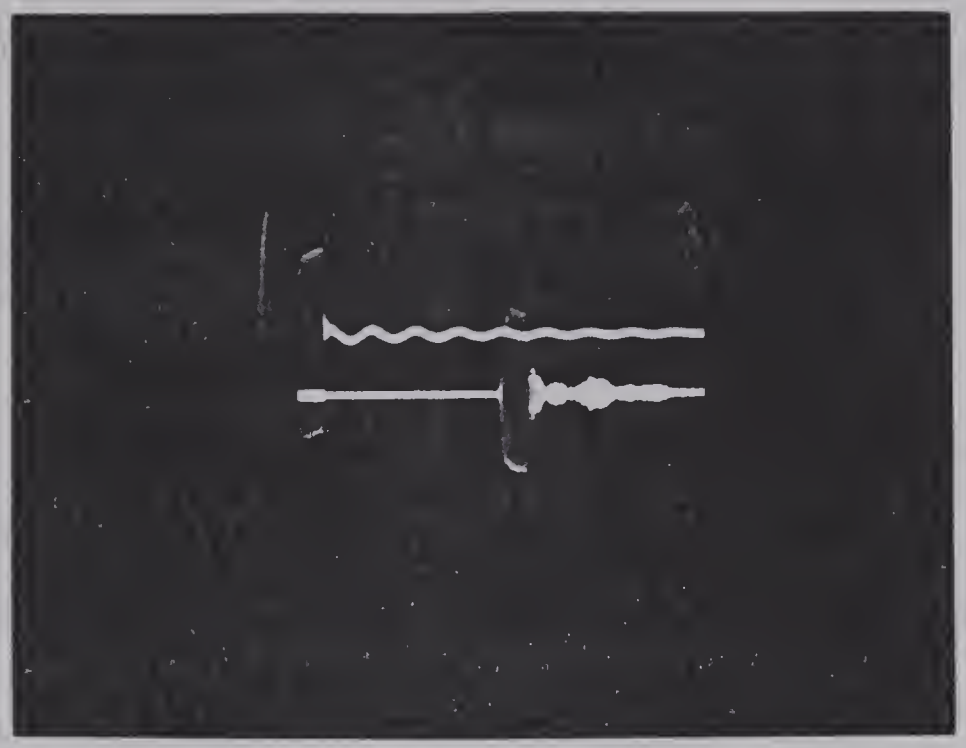

FIGURE 20

Oscilloscope trace illustrating electrical isolation of receiver and transmitter. The upper trace is the electrical signal applied to the transmitter while the lower trace is the received signal. Time separation between the two signals is due to the distance between the transmitter and the receiver and the velocity of sound. Echoes from the walls of the tank are apparent on the lower trace.

4.2.2. Phase versus azimuthal angle

For large distances from the radiating aperture the pressure is given by:

$$p = \frac{i\,\rho_o a^2 ck}{2r}\, U\, e^{i(\omega t - kr)}\, \frac{2\,J_1(k\,a\,\sin[\theta])}{k\,a\,\sin[\theta]}$$

As was mentioned in chapter 3 this equation illustrates that the phase of the radiation is expected to be that of a spherical wave, (e^{-ikr}). In order to test this two experiments were carried out. The first arrangement is illustrated in figure [21] and is fairly straightforward. The received acoustic wave was displayed on one channel of the CRT while the electrical wave used to drive the transducer was displayed on the other channel to provide a reference. The receiving element was rotated about the transmitting horn at a constant radius while the waves on the CRT were monitored. No phase shift was observed indicating that the phase dependence of the radiation is that of a spherical wave.

However, the mechanical scanning structure was not stable so that another experiment involving two transmitters was set up in order to further examine the phase dependence of the radiation from the horn. The basic geometry of the experiment which is shown in figure [22] is not critically dependent upon r. Unfortunately the results from this experiment are also dubious for reasons

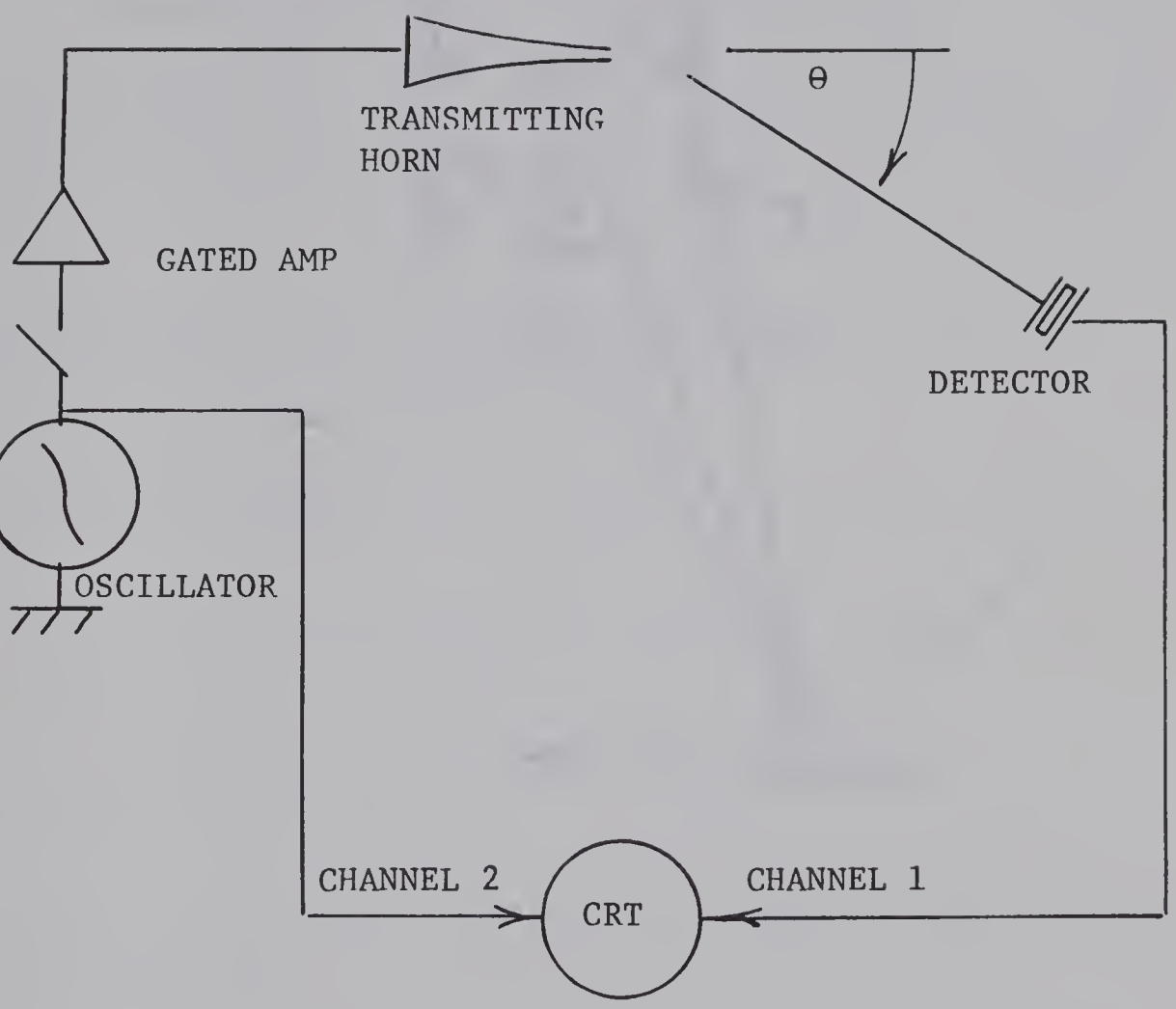

FIGURE 21

Experimental set up for first experiment to measure phase dependence

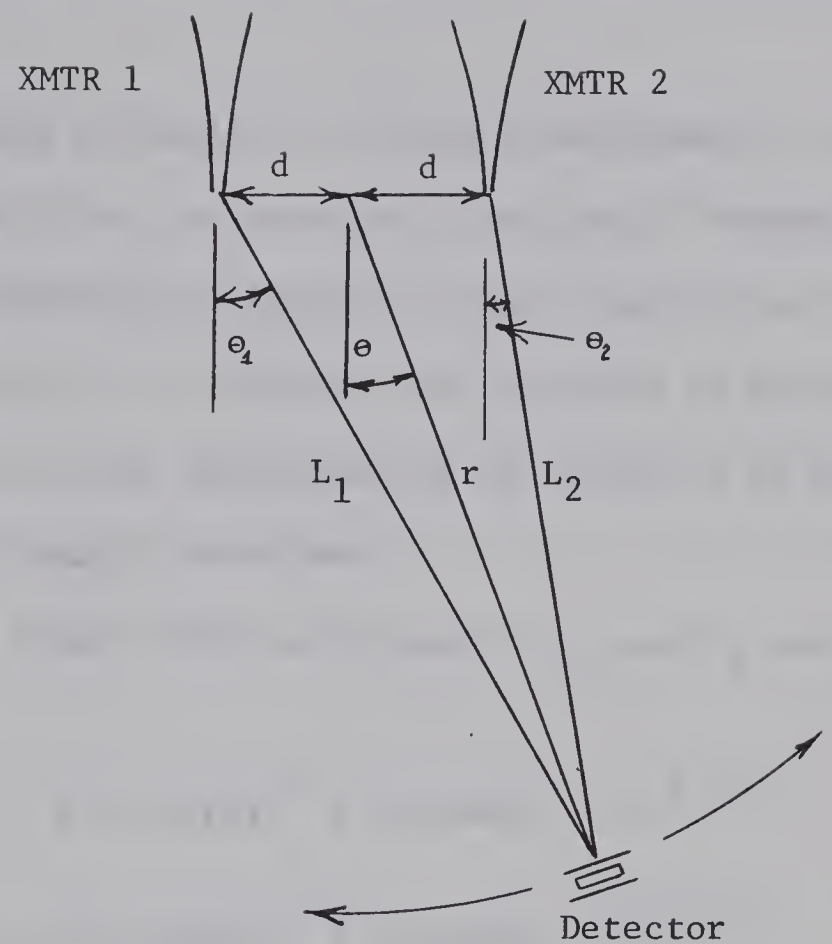

FIGURE 22

Geometry for the second experiment to measure phase dependence

which will be explained latter. This experiment is presented to illustrate some of the problems in making a phase measurement on the horns.

This experiment is similar to Young's experiment in that an interference pattern from two sources is recorded. However, the recording of the interference pattern is made over an arc instead of on a planer surface. In addition the recording is made over a much wider angle so that approximating the waves to be plane is not valid as in Young's experiment.

Referring to figure [22] the values of L_1 and L_2 are given by:

$$L_1 = L_1(r,\theta) = [(r\cos[\theta])^2 + (r\sin[\theta] + d)^2]^{1/2}$$

$$L_2 = L_2(r,\theta) = [(r\cos[\theta])^2 + (r\sin[\theta] - d)^2]^{1/2}$$

For L_1 and L_2 >> a then the amplitude profiles for horns one and two are given by:

$$D_1 = \frac{A_1\, J_1(k\ a\ \sin[\theta_1])}{L_1(k\ a\ \sin[\theta_1])}$$

$$D_2 = \frac{A_2\, J_1(k\ a\ \sin[\theta_2])}{L_2(k\ a\ \sin[\theta_2])}$$

Let the phase dependence be given by:

$$e^{-i(kL_1 + f_1(\theta_1))} = e^{i\phi_1}$$

$$e^{-i(k\ L_2 + f_2(\theta_2)} = e^{i\phi_2}$$

The time dependence, $e^{i\omega t}$, is not included here as it is not necessary for the analysis. The above expressions refer to horns one and two respectively. Note that the phase dependence is that of a spherical wave if the functions $f_1(\theta_1)$ and $f_2(\theta_2)$ are zero.

When L_1 and L_2 are sufficiently large so that the expressions for D_1 and D_2 are valid then the phasor ($Ae^{i\phi}$) of the radiation formed by the interference of the radiation from the two horns may be found by referring to figure [23]

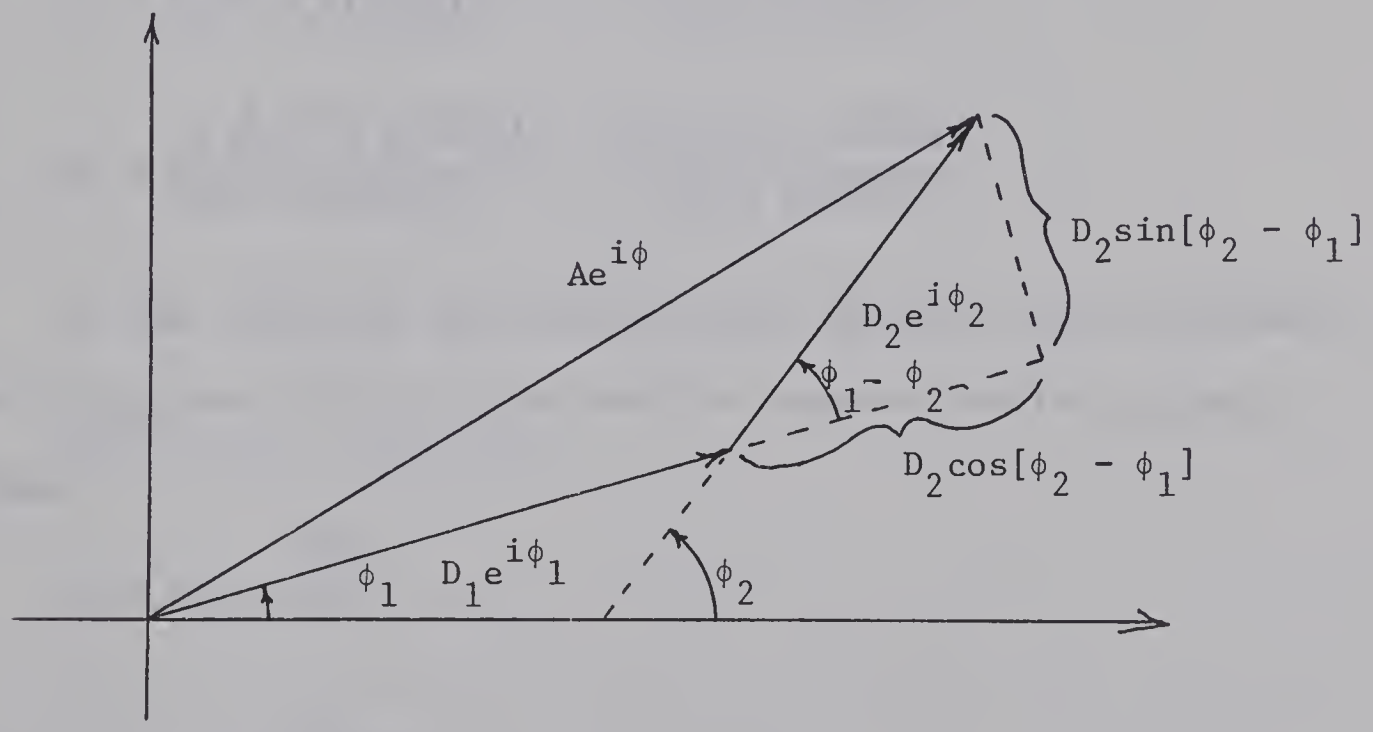

FIGURE 23

Phasor diagram used to calculate the interference pattern from two horns.

$$Ae^{i\phi} = D_1 e^{i\phi}1 + D_2 e^{i\phi}2$$

$$A = |Ae^{i\phi}| = \{(D_1 + D_2\cos[\phi_2 - \phi_1])^2 + (D_2\sin[\phi_2 - \phi_1])^2\}^{1/2}$$

It is this function that the experiment attempts to measure.

L_1 and L_2 and r have approximately the same direction θ if the position of the detector in space is such that $r >> d$. This being the case then $\theta_1 \cong \theta_2 \cong \theta$. L_1 and L_2 may be replaced by r in the denominator of the expressions for D_1 and D_2 if r is sufficiently large. Hence:

$$D_1 = \frac{A_1 J_1(k\ a \sin[\theta_1])}{L_1(k\ a \sin[\theta_1])} = \frac{A_1 J_1(k\ a \sin[\theta])}{r(k\ a \sin[\theta])}$$

$$D = \frac{A_2 J_1(k\ a \sin[\theta_2])}{L_2(k\ a \sin[\theta_2])} = \frac{A_2 J_1(k\ a \sin[\theta])}{r(k\ a \sin[\theta])}$$

If the radiation from the horns has spherical phase dependence then $f_1(\theta_1)$ and $f_2(\theta_2) = 0$ so that the expresssions for ϕ_1 and ϕ_2 become:

$$\phi_1 = kL_1 = \frac{2\pi L_1}{\lambda}$$

$$\phi_2 = kL_2 = \frac{2\pi L_2}{\lambda}$$

Hence:

$$A = \frac{J_1(k\ a \sin[\theta])}{r(k\ a \sin[\theta])} \left\{ \left[A_1 + A_2\cos\left((L_2 - L_1)\frac{2\pi}{\lambda} \right) \right]^2 + \left[A_2\sin\left((L_2 - L_1)\frac{2\pi}{\lambda} \right) \right]^2 \right\}^{1/2}$$

Experimental conditions correspond to holding r = R = 26.6 cm. = constant and varying θ from -30 to +30 degrees. The function A was evaluated for these conditions by means of the computer program in appendix (E). A comparison of the experimental and calculated results appears in figure [24]. The difference in the amplitude envelopes may be attributed to the directivity functions varying slightly from their expected values. A more serious discrepancy between the experimental and theoretical curve is that for increaseing θ the locations of the minima and maxima are not the same for the two curves.

These discrepancies in position of maxima and minima can not be attributed to variations in R from its nominal value of 26.6 cm. As was previously mentioned this experiment is not critically dependent upon R and this is indeed the case. By means of the computer the difference described below was calculated.

$$\frac{A(r=26.6,\theta)}{A(r=26.6,0)} - \frac{A(r=30,\theta)}{A(r=30,0)}$$

The greatest difference was less than 2×10^{-4}.

Since the horns are very similar in construction it seems reasonable to assume that the phase dependence for both horns is the same. In other words it would be reasonable to assume that $f_1(\theta) = f_2(\theta)$. Providing that $f_1(\theta)$ does not vary rapidly with

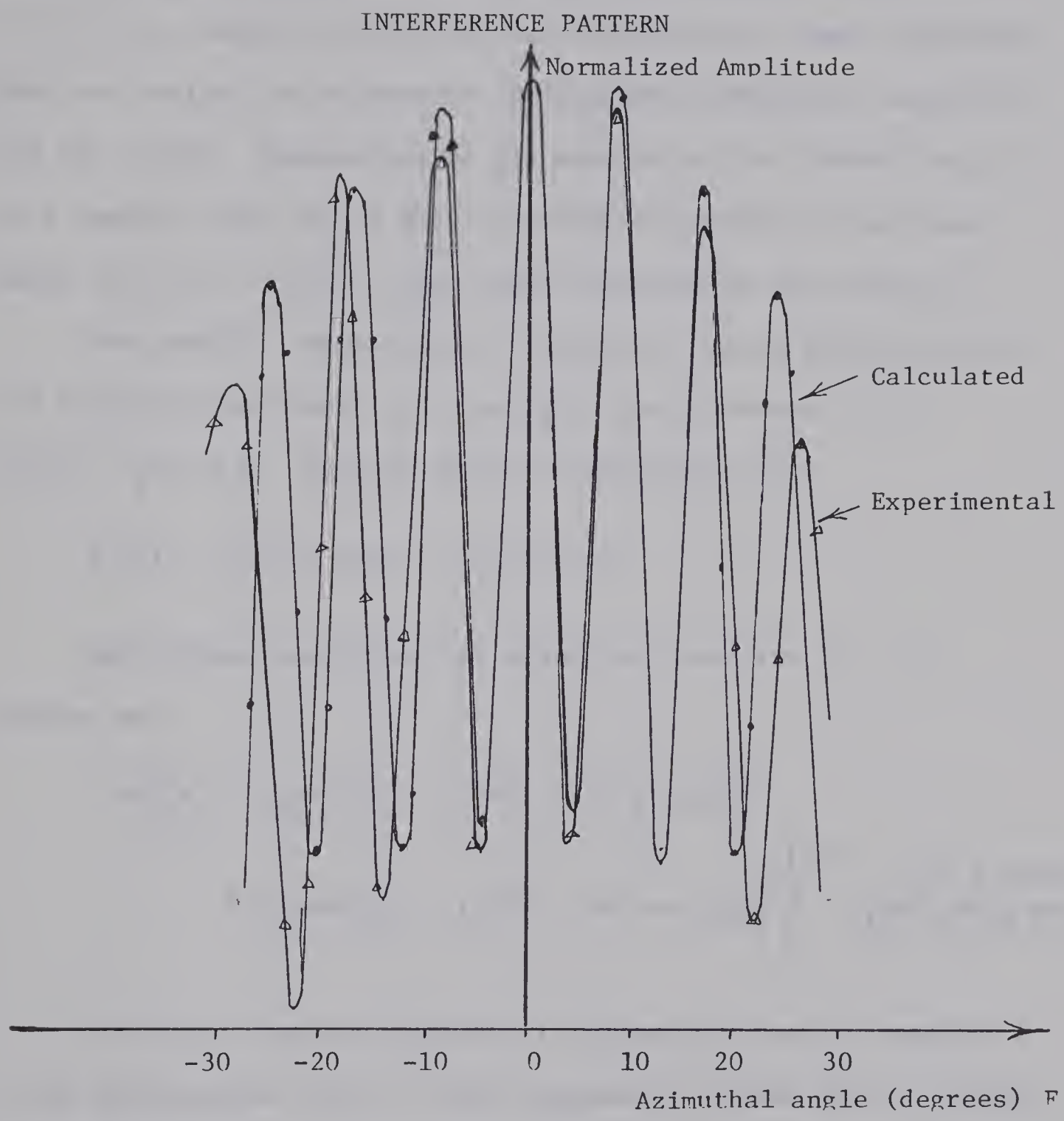

Figure 24

Interference pattern obtained from two radiating horns, compared to the interference pattern from two sources having spherical wave phase dependence. The radius of the arc the detector travelled was R = 26.6 cm.

θ then $f_1(\theta_1) = f_2(\theta_2) = f(\theta)$ because of the condition that $\theta \simeq \theta_1 \simeq \theta_2$. However this variation from spherical phase dependence does not explain the difference in locations between the maxima of the two curves. Examination of the expression for A shows that A is a function only of the phase difference between the two waves. Hence if $f_1(\theta_1) = f_2(\theta_2)$, then these functions do not affect A.

One possible explanation is that due to small differences in the horns the functions $f_1(\theta)$ and $f_2(\theta)$ are different, i.e., $f_1(\theta) - f_2(\theta) \neq 0$. For the sake of illustration let:

$$f_2(\theta) - f_1(\theta) = f(\theta) = -.85 \sin[\theta]$$

Under these conditions the normalized function for A is written as:

$$A = \left\{\left(A_1 + A_2\cos\left[(L_2 - L_1)\frac{2\pi}{\lambda} - .85 \sin[\theta]\right]\right)^2 + \left(A_2\sin\left[(L_2 - L_1)\frac{2\pi}{\lambda} - .85 \sin[\theta]\right]\right)^2\right\}^{1/2} \frac{J_1(k\ a \sin[\theta])}{(A_1 + A_2)(k\ a \sin[\theta])}$$

A plot of this curve appears in figure [25] and is compared to the experimental curve. Better agreement between the two curves in figure [25] than in figure [24] is noted.

Another possible source of error is that the scanning arc does not lie in the plane defined by the horn axis and the line joining the two apertures. Assuming the scanning arc to

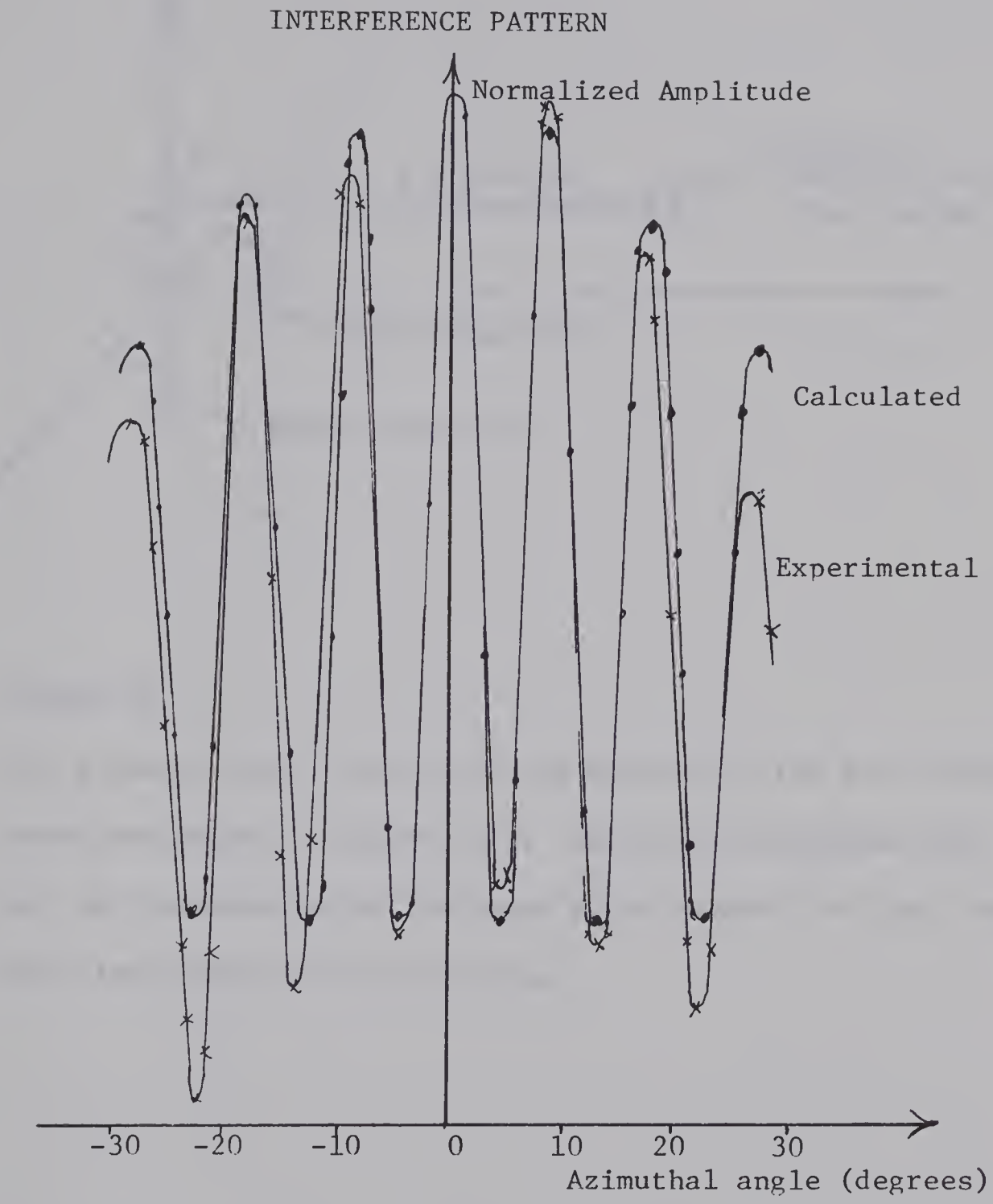

FIGURE 25

Interference pattern obtained from two radiating horns compared to two sources having the phase dependence described on page [52]

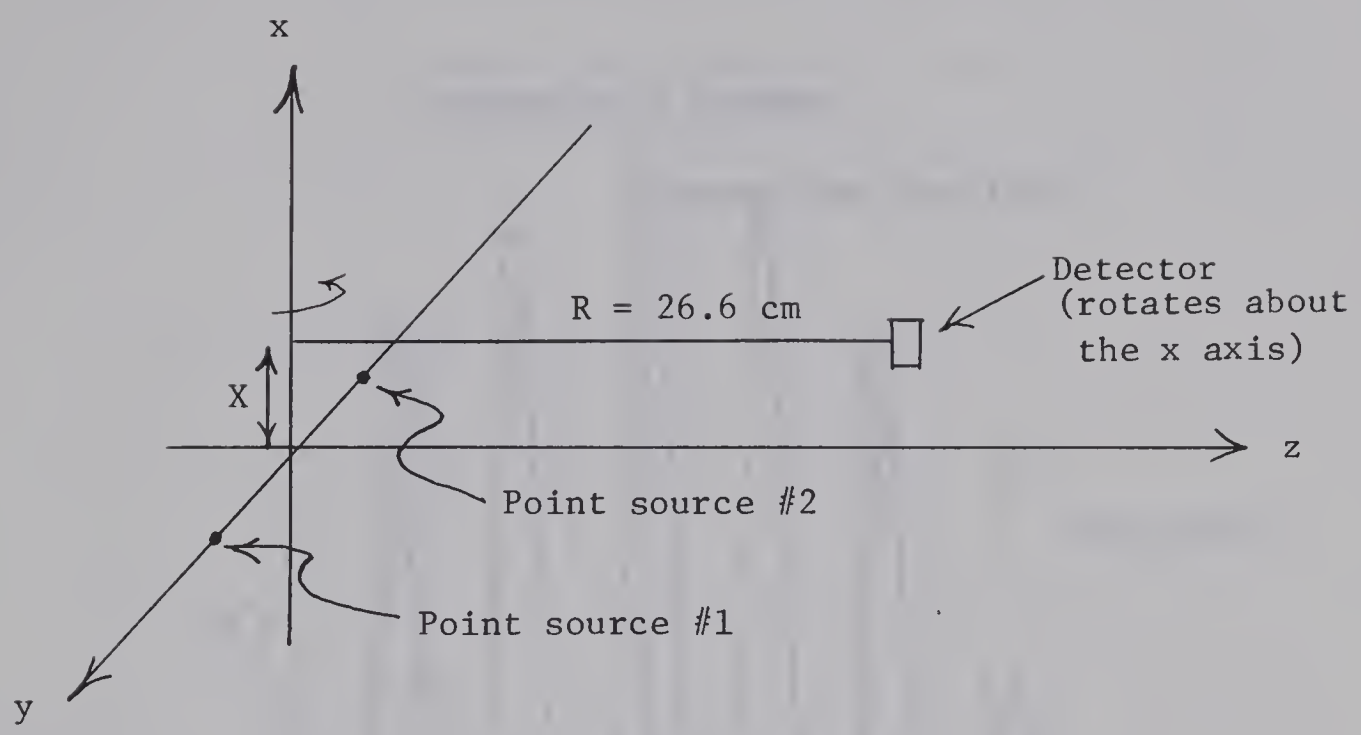

FIGURE 26

The geometry here illustrates the conditions for the "calculated" curve appearing in figure [27]. The plane containing the arc of the detector is displaced by an amount X = 5 cm. from the line joining the two sources.

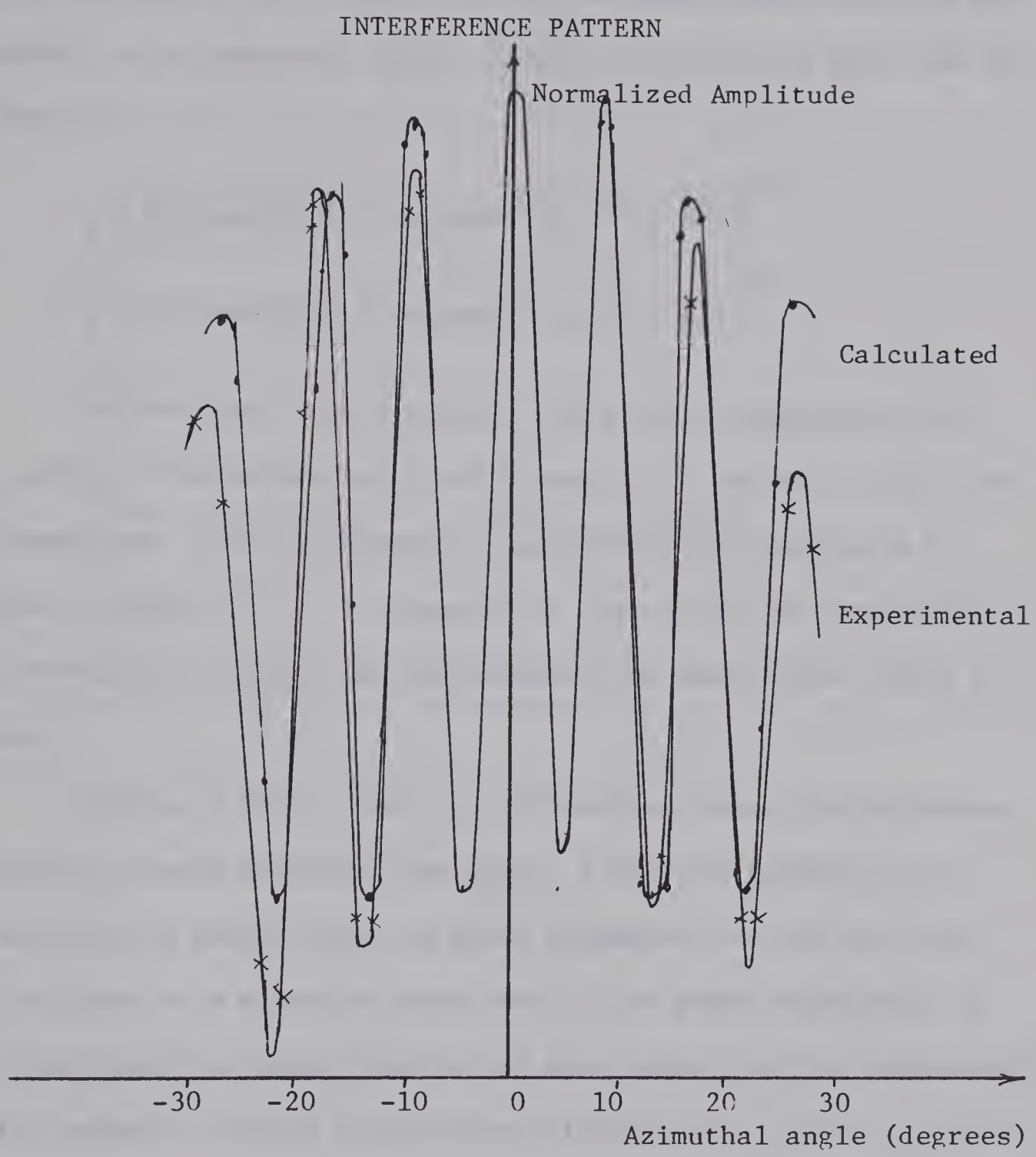

FIGURE 27

Interference pattern obtained from two radiating horns compared to the expected pattern under conditions illustrated in figure [26].

be defined as in figure [26] then the associated interference pattern would be as in figure [27]. The phase dependence has been assumed to be spherical $f_1(\theta) = f_2(\theta) = 0$. L_1 and L_2 in this case are given by:

$$L_1 = [(R\cos[\theta])^2 + (R\sin[\theta] + d)^2 + X^2)]^{1/2}$$

$$L_2 = [(R\cos[\theta])^2 + (R\sin[\theta] - d)^2 + X^2)]^{1/2}$$

The function A was evaluated using these expressions for L_1 and L_2. The values for X and R were X = 5 cm and R = 26.6 cm. A comparison of the experimental curve with the function A is given in figure [27]. If compared to figure [24] an improvement in correlation between the experimental and theoretical curve is noted.

Choosing X to be 5 cm is a bit extreme since the mechanical scanning is more accurate than that. With this in mind it is reasonable to assume that the phase dependence of the two horns is not that of a spherical wave, nor is the phase dependence of the two horns the same since it has been shown that the discrepancies which appear in figure [24] can be attributed to $f_2(\theta) - f_1(\theta) \neq 0$.

If the radiation characteristics of one of the sources were completely known (amplitude and phase) the radiation from the other could be uniquely determined from the interference pattern.

In other words, if one of the horns could be made to interfere with a plane wave emitted from a large flat crystal then the phase characteristics could be determined. Another alternative to obtaining accurate phase measurements is with the use of a scanning apparatus with sufficient stability so as to render the results of the first experiment accurate.

4.3 Horn and plane mounted transducer profile

A comparison of the radiation profile given by the horn device and that produced by a standard plane mounted piezoelectric crystal is shown in figure [28]. The improvement in performance characteristic is clearly illustrated in this diagram.

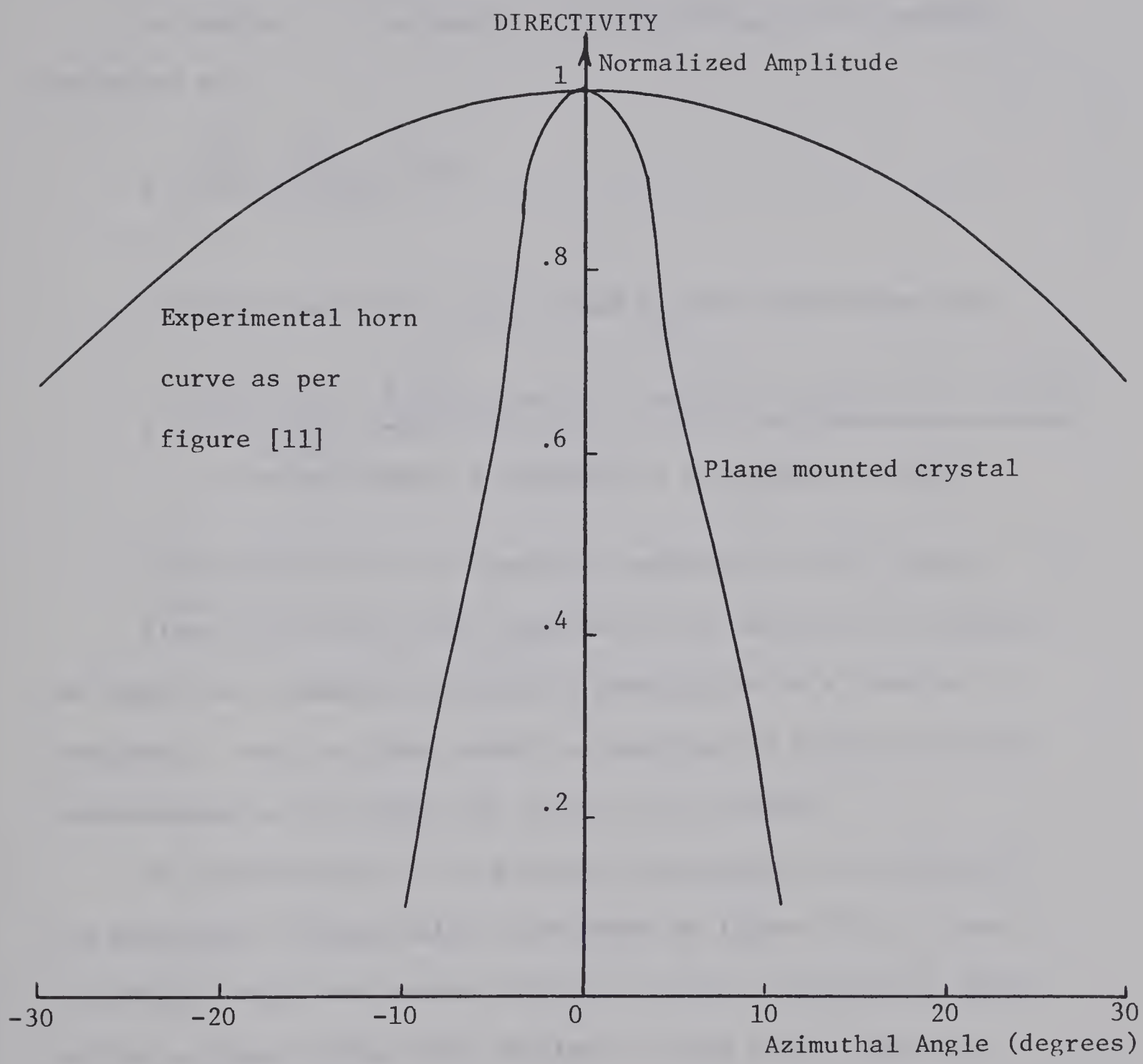

FIGURE 28

A comparison of directivity functions for a plane mounted crystal and a horn

4.4 Amplitude versus frequency

In chapter 3 an expression for the driving point impedance was given as:

$$Z = \frac{Z_1 Z_2 - M_{12}^2 + Z_1 Z_\ell}{Z_2 + Z_\ell}$$

If the values for Z_1, Z_2, Z_ℓ and M_{12} are substituted then:

$$Z = \frac{\rho_o{}^2 c^2 S_1 S_2 + i\left(\frac{\rho_o}{k}\right) c S_1 \{(m/2) - \beta\cot[\beta\ell]\}\{\rho_o c S_2 [R(x) + iX(x)]\}}{-\frac{i\rho_o c S_2}{k}((m/2) + \beta\cot[\beta\ell]) + \rho_o c S_2 [R(x) + iX(x)]}$$

Note that this is the impedance presented to the crystal.

Since the driving point impedance is a function of frequency we expect the transmitted intensity should also be a function of frequency. Such an effect should be manifest as a fine structure superimposed on the normal "Q" curve of the crystal.

An investigation of this effect was carried out by means of the experiment schematically illustrated in figure [29]. Plots of transmitted amplitude versus frequency for the crystal-horn device and for a plane crystal were obtained. These curves appear in figure [30].

Also appearing in figure [30] is a calculated curve for amplitude versus frequency. This curve was obtained by evaluating

the real part of the function for Z, ie. the real part of the impedance presented to the crystal. This result was then multiplied by the envelope of the experimental curve which appears in figure [30]. The computer program used to carry out the calculation appears in appendix (F).

The spacing between the amplitude peaks is determined by the term $\beta\ell$. An increment of π in $\beta\ell$ corresponds to the spacing between two adjacent amplitude peaks. These results indicate that the horn may be 'tuned' simply by translation of the transducer slightly along the horn axis. The ability to tune each structure is a highly desirable feature from a system point of view as it means that only one master driving oscillator is necessary for many horns.

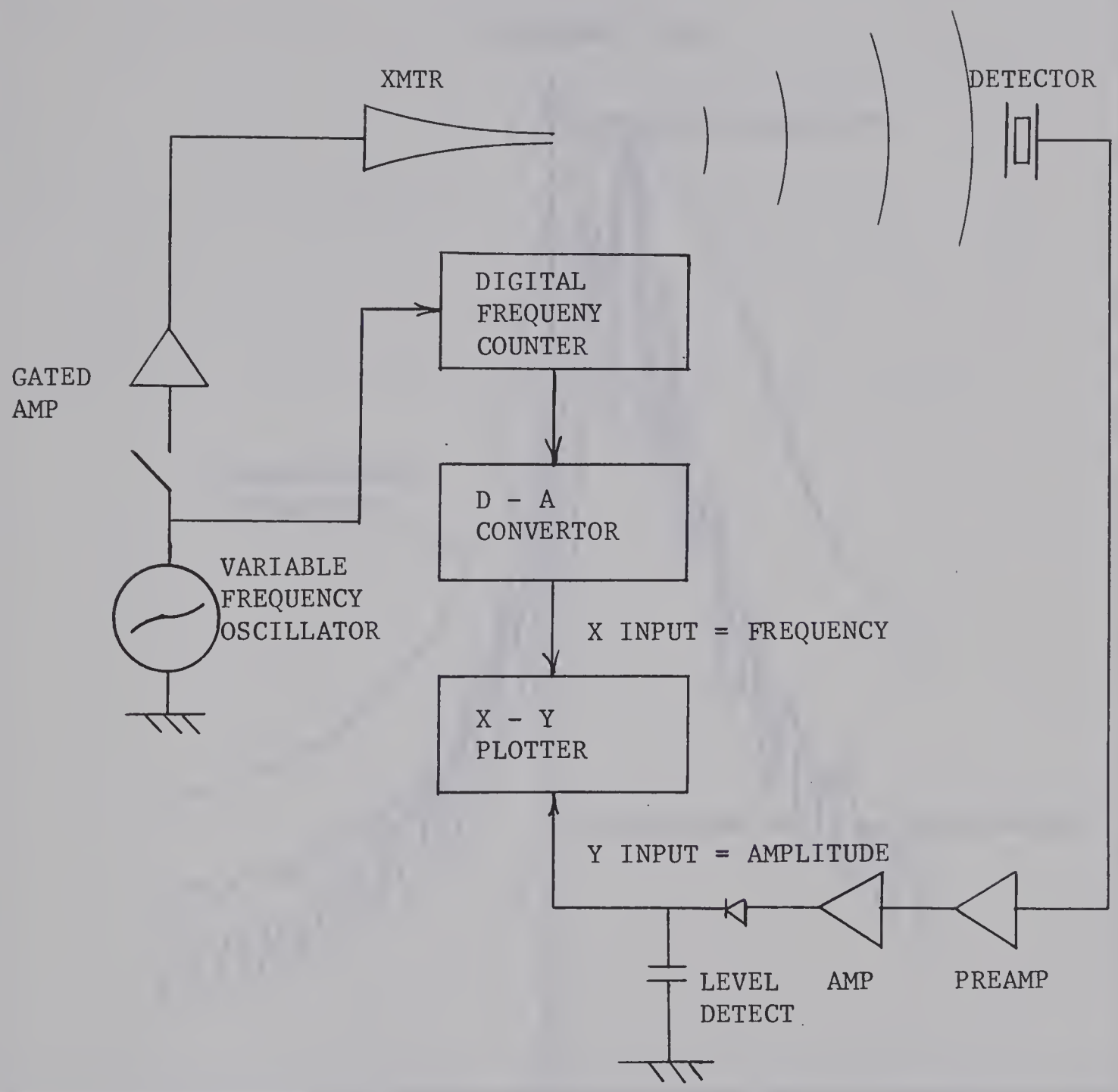

FIGURE 29

Schematic of experiment to obtain frequency versus amplitude plot

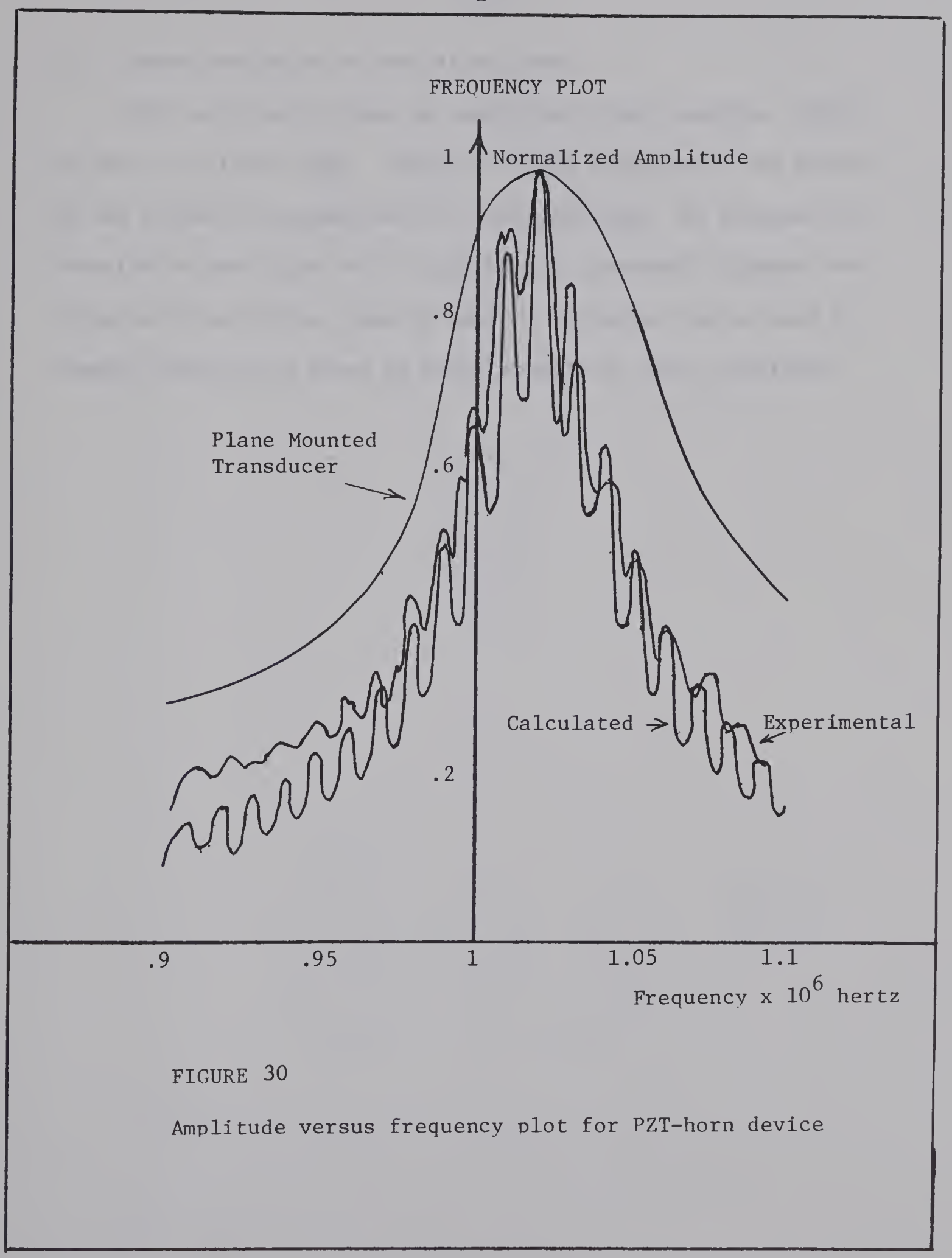

FIGURE 30

Amplitude versus frequency plot for PZT-horn device

4.5 Characteristics of horn in an array

The horns may be bent to facilitate close mounting. This is shown in figure [31]. The next figure illustrates the effect on the radiation pattern due to close mounting. An increase in directivity over that of a single horn is observed although for fields of view of less than 15 degrees the horns can be used to closely simulate an array of point sources or point receivers.

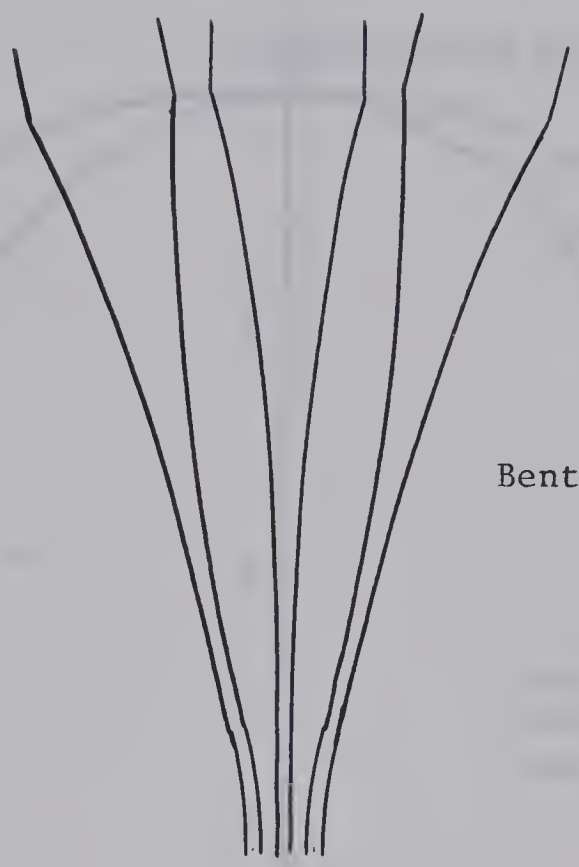

Bent Horns

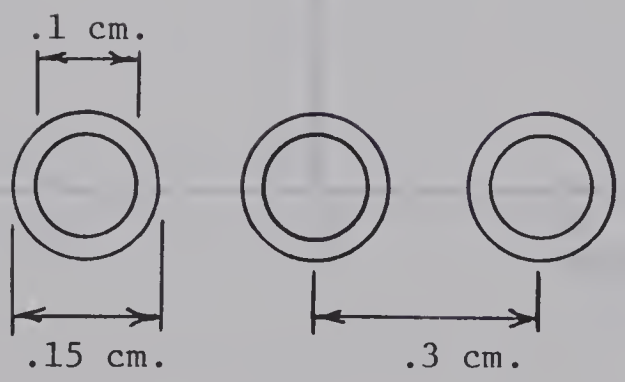

Aperture
Spacing
Details

FIGURE 31

Close mounting details to facilitate simulation of point source array

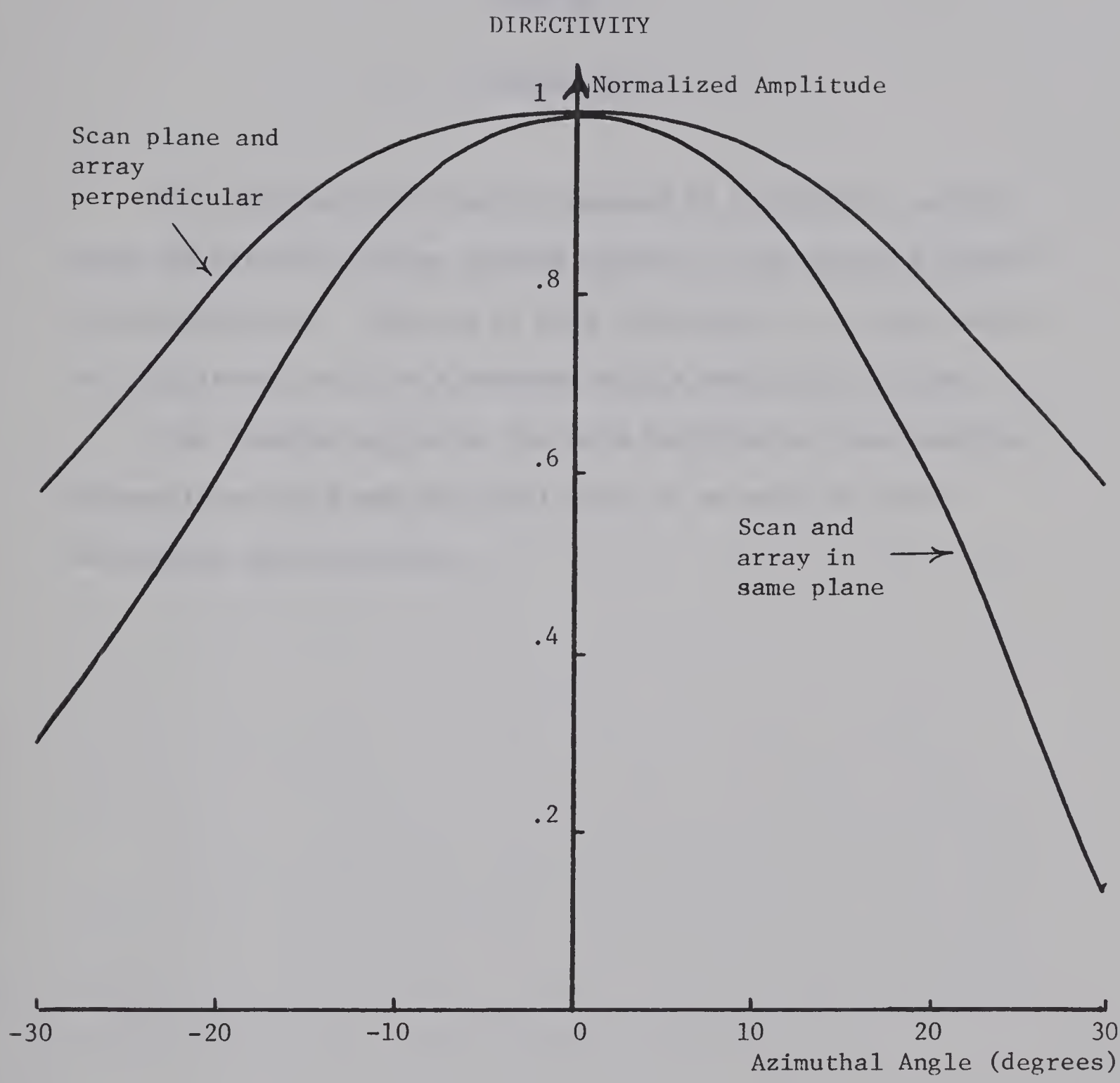

FIGURE 32

Directivity plot for horn mounted in an array

CHAPTER 5

CONCLUSIONS

The experimental results presented in this thesis indicate that the PZT-horn devices perform closely to the expected theoretical predictions. They may be used effectively as a point source of high intensity or as a receiver with a wide field of view.

The flexible nature of the horn facilitates close mounting of apertures and hence the fabrication of an array of point sources or point receivers.

CHAPTER 6

SUGGESTIONS FOR FURTHER WORK

The very positive experimental results obtained from the horn described in this thesis warrant further investigation into inverse horns.

Different flare constants and aperture sizes should be tried. A conical horn would be much easier to fabricate than an exponential horn and should be investigated.

Materials other than copper could be used. Perhaps a more rigid material would stop the horn aperture from vibrating and a wider field of view would be obtained. If horns were fabricated by glass blowing then very small apertures could be obtained and the horn would be effective as a point source at higher frequencies.

This thesis has shown that it is possible to use the horn in an array so that is is feasible to realize the linear crossed-array holographic system proposed by Wells. Such a system is presently under construction at the University of Alberta.

APPENDIX A

ELECTROFORMING DETAILS

A.1 Mandrel preparation

For cleaning and easy removal of electroformed horns from the stainless steel mandrel the mandrel was treated cathodically in a 6 oz. / gal. solution of trisodium phosphate in water. The temperature of the solution was between 140 and 180 degrees Farenhiet. A current of 50 amp / ft^2 for one minute was used and then the mandrel was rinsed in water at 100 degrees F.

A.2 Electroforming solution

The electroforming solution consisted of 30 oz. / gal. of copper sulfate and 6 oz. / gal. of sulfuric acid. A current density of 100 amps / ft^2 or about .5 amps per mandrel was used. The solution was maintained at a temperature of 80 degrees F and was constantly circulated about the mandrel.

APPENDIX B

VELOCITY POTENTIAL

B.1 Preliminaries

This appendix follows closely reference [15].

For small increments of density a term called condensation ($\hat{s}$) is defined as:

$$\hat{s} = \frac{\delta\rho}{\rho_o}$$

$$\rho = \rho_o + \delta\rho = \rho_o(1 + \hat{s}) \qquad \text{(b.1)}$$

since $\rho v = \rho_o v_o$

we have $\hat{s} = -\frac{\delta v}{v_o}$ (b.2)

v = specific volume

ρ = density

v_o = mean specific volume

ρ_o = mean density

For an adiabatic fluid which behaves as described by:

$$P_1 V_1^{\gamma} = P_o V_o^{\gamma}$$

P_1 = pressure at V_1

P_o = initial pressure

V_1 = volume at P_1

V_o = initial volume

the following relationship holds:

$$\frac{\delta P}{P_o} = -\frac{\gamma \delta v}{v_o} = \gamma \hat{s}$$

Defining k', coefficient of cubic elasticity, as

$$k' = \gamma P_o = \frac{\delta P}{\hat{s}} \qquad (b.3)$$

then $P_1 = P_o + k'\hat{s} = P_o + \delta P$

B.2 Equation of continuity

Next the equation of continuity is derived.

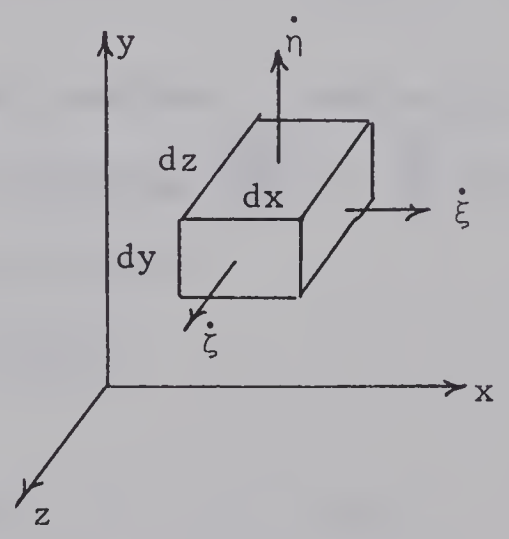

Considering flow in the x direction through the volume element the expression for the net flux is:

$$\delta t \left[\rho\dot{\xi} - (\rho\dot{\xi} + \frac{\partial(\rho\dot{\xi})}{\partial x} dx) \right] A = - Adx \frac{\partial(\rho\dot{\xi})}{\partial x} \partial t$$

where A = dy dz

The increase in the amount of fluid contained in the element is given by:

$$\delta t \; A \; dx \; \frac{\partial \rho}{\partial t}$$

hence the equation:

$$\frac{\partial \rho}{\partial t} + \frac{\partial (\rho \dot{\xi})}{\partial x} = 0 \qquad \text{(b.4)}$$

using $\rho = \rho_o(1 + \hat{s})$ and realizing that $\frac{\partial (\hat{s}\dot{\xi})}{\partial x} << \frac{\partial \dot{\xi}}{\partial x}$

then:

$$\frac{\partial \hat{s}}{\partial t} + \frac{\partial \dot{\xi}}{\partial x} = 0 \qquad \text{(b.5)}$$

The above is the equation of continuity.

The validity of assuming $\frac{\partial (\hat{s}\dot{\xi})}{\partial x} << \frac{\partial \dot{\xi}}{\partial x}$ is verified later by equations (b.25) and (b.26).

From (b.5) we obtain:

$$\frac{\partial^2 s}{\partial t \partial x} + \frac{\partial^2 \dot{\xi}}{\partial x^2} = 0 \qquad \text{(b.6)}$$

B.3 Force equation

Equating the net force on the element to the rate of change of momentum of the element in the x direction one obtains:

$$dx \; dy \; dz \; (\frac{\partial p}{\partial x} + \rho \ddot{\xi}) = 0 \qquad \text{(b.7)}$$

Here p is the excess pressure; $\delta P = p = k's$ (b.8)

Substituting for p the equation for force becomes

$$k' \frac{\partial \hat{s}}{\partial x} + \rho \ddot{\xi} = 0 \qquad \text{(b.9)}$$

The next step is differentiation with respect to time and the use of the approximation that $\frac{\partial \dot{\xi}}{\partial t} >> \frac{\dot{\xi} \partial \dot{\xi}}{\partial x}$.

This approximation is considered in reference [16] and is valid for waves in which $\frac{\dot{\xi}}{c} << 1$. Referring to equation (b.24) we see that $\frac{\dot{\xi}}{c} < 10^{-4} << 1$

$$k' \frac{\partial^2 \hat{s}}{\partial x \partial t} + \rho \frac{\partial^2 \dot{\xi}}{\partial t^2} = 0$$

By comparison of this equation to (b.6) the result is the wave equation.

$$\frac{\partial^2 \dot{\xi}}{\partial t^2} = \frac{k'}{\rho} \frac{\partial^2 \dot{\xi}}{\partial x^2} \qquad \text{(b.10)}$$

$$\text{Hence } c^2 = \frac{k'}{\rho} \qquad \text{(b.11)}$$

where c is the velocity of propagation.

B.4 Velocity potential

Previously the expression for forces in the x direction was given as:

$$\rho \ddot{\xi} = - \frac{\partial p}{\partial x}$$

Using $p = k'\hat{s}$ and $c^2 = k'/\rho$ expressions for the three directions are obtained as:

$$\ddot{\xi} = - c^2 \frac{\partial \hat{s}}{\partial x} \qquad (b.12)$$

$$\ddot{\eta} = - c^2 \frac{\partial \hat{s}}{\partial y} \qquad (b.13)$$

$$\ddot{\zeta} = - c^2 \frac{\partial \hat{s}}{\partial z} \qquad (b.14)$$

To simplify the theory a single function called the velocity potential (ϕ) which contains all three displacement quantities ζ, η and ξ is sought. For a fluid in which there is no circulation a function ϕ exists such that:

$$\dot{\xi} = - \frac{\partial \phi}{\partial x} \qquad (b.15)$$

$$\dot{\eta} = - \frac{\partial \phi}{\partial y} \qquad (b.16)$$

$$\dot{\zeta} = - \frac{\partial \phi}{\partial z} \qquad (b.17)$$

or $\phi = - \int (\dot{\xi} dx + \dot{\eta} dy + \dot{\zeta} dz)$

Integration of the equations (b.12), (b.13) and (b.14) yields:

$$\dot{\xi} = - c^2 \frac{\partial}{\partial x} \int \hat{s} dt + \xi_o$$

$$\dot{\eta} = - c^2 \frac{\partial}{\partial y} \int \hat{s} dt + \dot{\eta}_o$$

$$\dot{\zeta} = - c^2 \frac{\partial}{\partial z} \int \hat{s} dt + \dot{\zeta}_o$$

where ζ_o, $\dot{\eta}_o$ and $\dot{\xi}_o$ are velocities at $t = 0$. Assuming these

velocities to be as $\dot{\xi}_o = -\frac{\partial \phi_o}{\partial x}$ we have:

$$\phi = c^2 \int \hat{s}\, dt + \phi_o$$

differentiating we have:

$$\dot{\phi} = c^2 \hat{s} \qquad (b.18)$$

In one dimension it has been shown that the equation of continuity (b.5) can be written as:

$$\frac{\partial \hat{s}}{\partial t} + \frac{\partial \dot{\xi}}{\partial x} = 0 \qquad (b.19)$$

A simple extension to three dimensions results in:

$$\frac{\partial s}{\partial t} + \frac{\partial \dot{\xi}}{\partial x} + \frac{\partial \dot{\eta}}{\partial y} + \frac{\partial \dot{\zeta}}{\partial z} = 0 \qquad (b.20)$$

Substitution of equations (b.15), (b.16), (b.17) and (b.18) along with the approximation $\dot{\phi} \cong \frac{\partial \phi}{\partial t}$ (reference [16]) yields:

$$\frac{\partial^2 \phi}{\partial t^2} - c^2 \nabla^2 \phi = 0$$

B.5 The validity of $\frac{\partial \dot{\xi}}{\partial x} >> \frac{\partial (\dot{\xi} \hat{s})}{\partial x}$

In order to check the validity of the approximation that $\frac{\partial \dot{\xi}}{\partial x} >> \frac{\partial (\dot{\xi} \hat{s})}{\partial x}$ an examination of a plane wave is carried out.

For a plane wave travelling in the x direction:

$$\frac{\partial^2 \phi}{\partial t^2} - c^2 \frac{\partial^2 \phi}{\partial x^2} = 0$$

The solution is:

$$\phi = A\, e^{i(\omega t - kx)}$$

Hence

$$\dot{\xi} = -\frac{\partial \phi}{\partial x} = ikA\, e^{i(\omega t - kx)} \qquad (b.21)$$

$$\xi = \int \dot{\xi}\, dt = \frac{k}{\omega} A\, e^{i(\omega t - kx)} \qquad (b.22)$$

A relationship between ξ (displacement) and $\hat{s}$ (condensation) is derived.

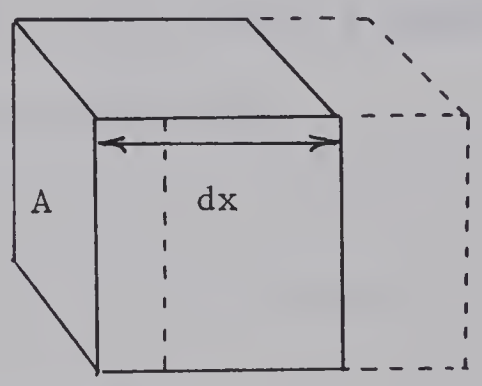

$$\hat{s} = -\frac{\delta v}{v_o}$$

$$\delta v = (dx + \frac{\partial \xi}{\partial x} dx)A - A\, dx$$

$$v_o = A\, dx$$

$$\hat{s} = -\frac{\partial \xi}{\partial x}$$

$$\hat{s} = \frac{ik^2}{\omega} A\, e^{i(\omega t - kx)} = ik\, \xi \qquad \text{(b.23)}$$

If the wave exists in water at a depth of less than one meter it would be impossible to have partial pressures as high as one atmosphere because of cavitation.

$$\delta P < 1.013 \times 10^5 \text{ NT./M}^2$$

$$\delta P = k'\hat{s} \qquad \text{(b.8)}$$

Kinsler and Frey [17] define a quantity called the isothermal bulk modulus (B_t) of a fluid by:

$$B_t = \frac{c^2 \rho_o}{\gamma}$$

From (b.11) we have:

$$c^2 = \frac{k'}{\rho} \cong \frac{k'}{\rho_o}$$

so that $k' = \gamma B_t$

Values for γ and B_t are listed in reference [18] as:

$$\gamma = 1.004$$

$$B_t = 2.18 \times 10^9 \text{ NT./M}^2$$

Hence $k' = 2.19 \times 10^9$ NT./M^2 for water.

Now an upper bound may be placed on the magnitude of $\hat{s}$.

$$|\hat{s}| < \frac{1.013 \times 10^5}{2.19 \times 10^9} = .463 \times 10^{-4}$$

$$\dot{\xi} = i\omega\xi$$

$$c = \omega/k$$

Hence by equation (b.23) we have

$$\dot{\xi} = c\hat{s} \tag{b.24}$$

For P = 1 ATM. we have:

$$\frac{\partial\dot{\xi}}{\partial x} = -ick\hat{s} = (-ick)(.463 \times 10^{-4})e^{i(\omega t - kx)} \tag{b.25}$$

$$\frac{\partial(\dot{\xi}\hat{s})}{\partial x} = \frac{\partial(c\hat{s}^2)}{\partial x} = (-ick)(.43 \times 10^{-8})e^{2i(\omega t - kx)} \tag{b.26}$$

The magnitude of $\frac{\partial\dot{\xi}}{\partial x}$ is much greater than that of $\frac{\partial(\dot{\xi}\hat{s})}{\partial x}$ so the approximation $\frac{\partial(\dot{\xi} + \dot{\xi}\hat{s})}{\partial x} \cong \frac{\partial\dot{\xi}}{\partial x}$ is valid. Note also that $\hat{s}\dot{\xi} << \dot{\xi}$ and $\frac{\dot{\xi}}{c} << 1$, two other approximations used in this appendix.

B.6 Velocity potential in the horn

An approximate equation describing the velocity potential within the horn is now discussed. The approximations used are

discussed in reference [19].

The equation for velocity potential which is used to describe wave motion in the horn is derived by assuming that the waves in the horn are plane and propagate in the direction defined by the axis of the horn. A short explanation of this assumption is given.

Consider a curvilinear coordinate system as shown below.

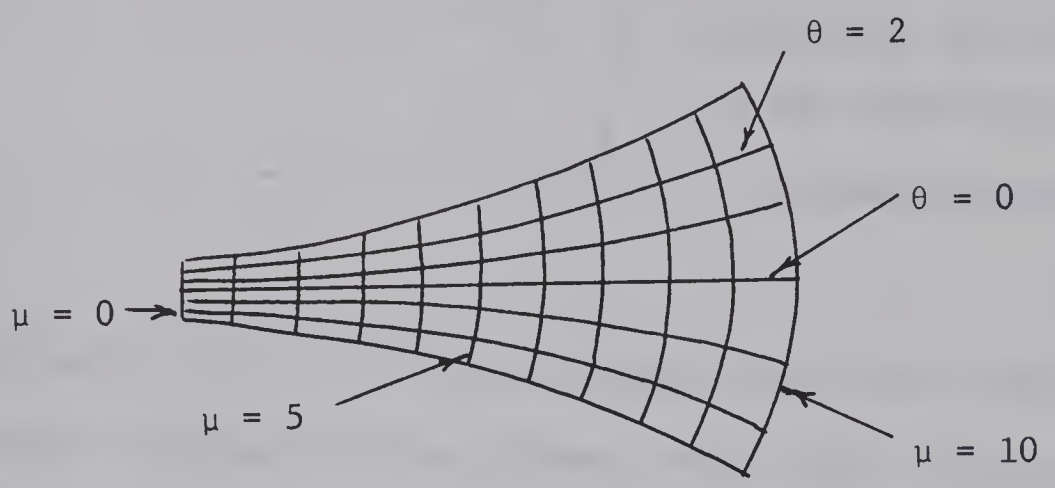

Lines of constant μ are perpendicular to lines of constant θ. The distance between two lines of constant μ is not a constant but is dependent on θ.

If the horn did not flare rapidly then one would expect that waves would propagate in the direction defined by lines of constant θ. In this case deriving an expression for the velocity potential would involve solving the equation of continuity and the

the force equation for the element shown below.

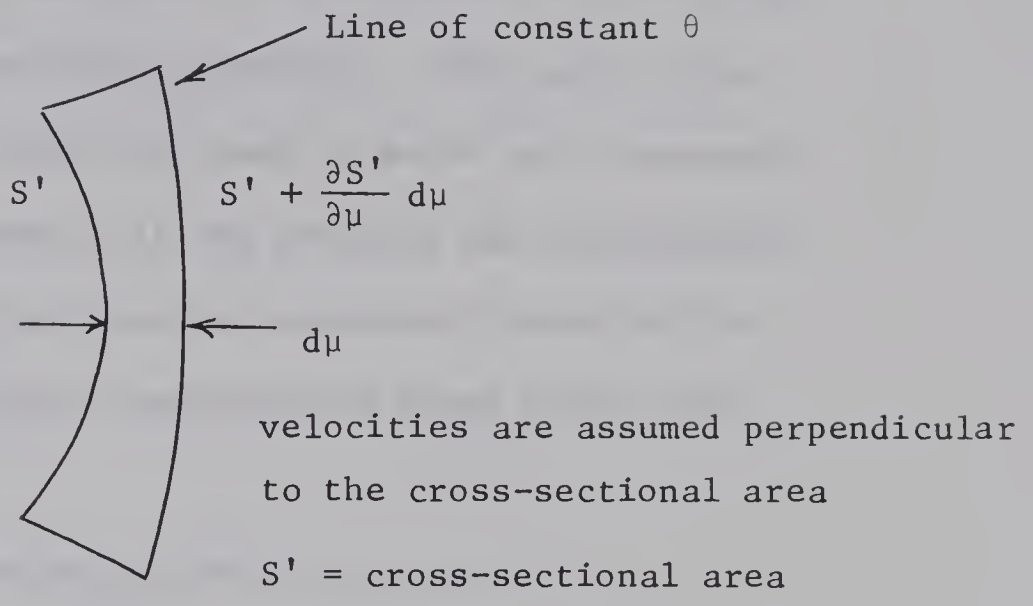

For horns which do not flare rapidly the term dμ would be essentially a constant for the element shown above (reference [20]).

Writing the equations for continuity and force in this curvilinear system is difficult because of the dependence of dμ on θ and because there is no simple expression for cross-sectional area. To circumvent this problem a rectangular coordinate system is used. The waves are assumed to travel in the x direction only.

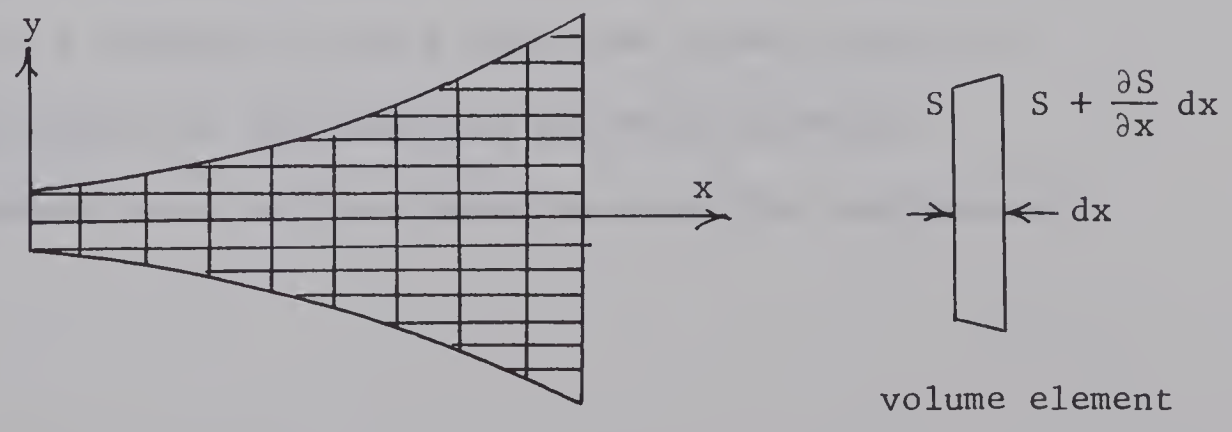

For horns which do not flare rapidly $dx = d\mu$, $S = S'$ and $\frac{\partial S}{\partial x} dx = \frac{\partial S'}{\partial \mu} d\mu$. Under these conditions the equations for continuity and force would appear mathematically identical. The case of the plane wave approximation is relatively easy to solve and accurately describes the amplitude dependence of the pressure and displacement velocity. However, the solution does not accurately describe the direction of propagation or phase dependence of waves within the horn.

In reference [2] P.M. Morse claims that plane wave approximation is valid for horns satisfying the condition $|\frac{r_s}{2m}| << 1$. For the horn used is this thesis $|\frac{r_s}{2m}| = .03$. The term r_s is the radius of the small end of the horn.

In defence of the approximations used it can be said that the wave entering the large end of the horn is plane and at the smaller end the velocity should be in the direction of the x axis since at the boundary velocities must be tangential to the horn surface which is almost parallel to the horn axis. On the axis the velocities are in the x direction by symmetry arguments. Recall too that the horn aperture is only a fraction of a wavelength in radius so that a velocity in the y direction is not likely to exist in the section of the horn near the small aperture.

The approach used in this thesis to solve for the velocity

potential of the horn does not lead to an exact solution but as exact solution is, the author feels, beyond the scope of this thesis.

The equation of continuity for the plane wave approximation is now derived

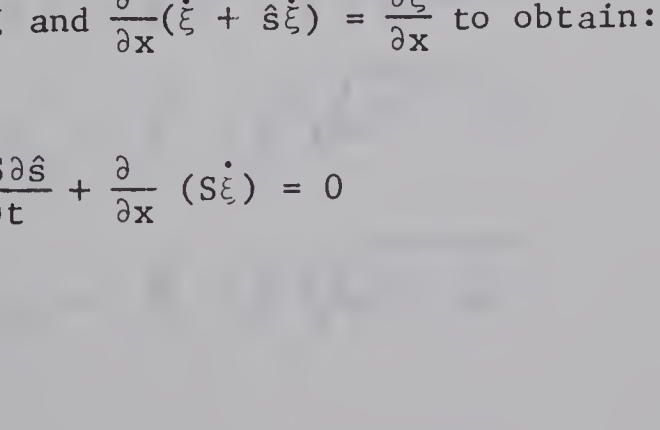

S = cross-sectional area

$= S_1 e^{(mx/2)}$

For details of horn geometry consult figure 2.

$$\delta t\left(\frac{\partial \rho}{\partial t}\right) S dx = \delta t\left[\rho\dot{\xi}S - \left(\rho\dot{\xi} + \frac{\partial(\rho\dot{\xi})}{\partial x} dx\right)\left(S + \frac{\partial S}{\partial x} dx\right)\right]$$

$$-\left(\frac{\partial \rho}{\partial t}\right) S\, dx = \rho\dot{\xi}\,\frac{\partial S}{\partial x} dx + S\,\frac{\partial(\rho\dot{\xi})}{\partial x} dx + \left(\frac{\partial(\rho\dot{\xi})}{\partial x}\right)\left(\frac{\partial S}{\partial x}\right) d^2x$$

Ignoring second order quantities we have:

$$-\frac{\partial \rho S}{\partial t} = \frac{\rho\dot{\xi}\partial S}{\partial x} + \frac{S\partial(\rho\dot{\xi})}{\partial x}$$

Substitute $\rho = \rho_o(1 + \hat{s})$ and use the approximations $\hat{s}\dot{\xi} << \dot{\xi}$ and $\frac{\partial}{\partial x}(\dot{\xi} + \hat{s}\dot{\xi}) = \frac{\partial \dot{\xi}}{\partial x}$ to obtain:

$$\frac{S\partial \hat{s}}{\partial t} + \frac{\partial}{\partial x}(S\dot{\xi}) = 0 \qquad \text{(b.27)}$$

The approximations used were previously examined and justified for the case of plane waves. Another examination will not be carried out for waves in the horn but rather the previous results will be used. Recall equations b.18 and b.15.

$$\dot{\phi} = c^2 \hat{s}$$

$$\dot{\xi} = - \frac{\partial \phi}{\partial x}$$

These are substituted in b.27 to obtain:

$$\ddot{\phi} = c^2 \frac{\partial \phi}{\partial x} \frac{\partial \ln S}{\partial x} + c^2 \frac{\partial^2 \phi}{\partial x^2} \qquad \text{(b.28)}$$

For periodic oscillations $\ddot{\phi} = -\omega^2 \phi$

$$\left[\frac{\partial^2}{\partial x^2} + m \frac{\partial}{\partial x} + k^2 \right] \phi = 0$$

where m = flare constant

k = wave number

This has the solution

$$\phi = [A' e^{u_1 x} + B' e^{u_2 x}] e^{i\omega t}$$

$$u_1 = - \frac{m}{2} + \frac{i}{2} \sqrt{4k^2 - m^2}$$

$$u_2 = - \frac{m}{2} - \frac{i}{2} \sqrt{4k^2 - m^2}$$

ϕ is the velocity potential and is the equation used in chapter 3. The velocity components are found from ϕ by

$$\left.\begin{aligned} \dot{\xi} &= -\frac{\partial \phi}{\partial x} \\ \dot{\eta} &= -\frac{\partial \phi}{\partial y} \\ \dot{\zeta} &= -\frac{\partial \phi}{\partial z} \end{aligned}\right\} \quad \text{These two terms are 0 for the horn.}$$

The excess pressure is found by:

$$p = \rho\dot{\phi} \cong \rho_o\dot{\phi}$$

APPENDIX C

ELECTRICAL CIRCUITS

C.1 Low noise preamplifier

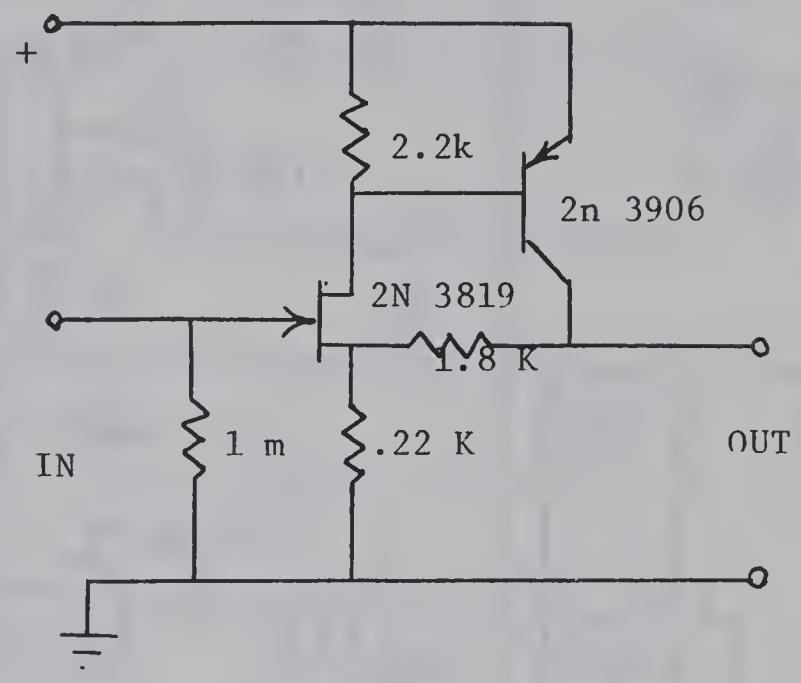

C.2 Gated Amplifier

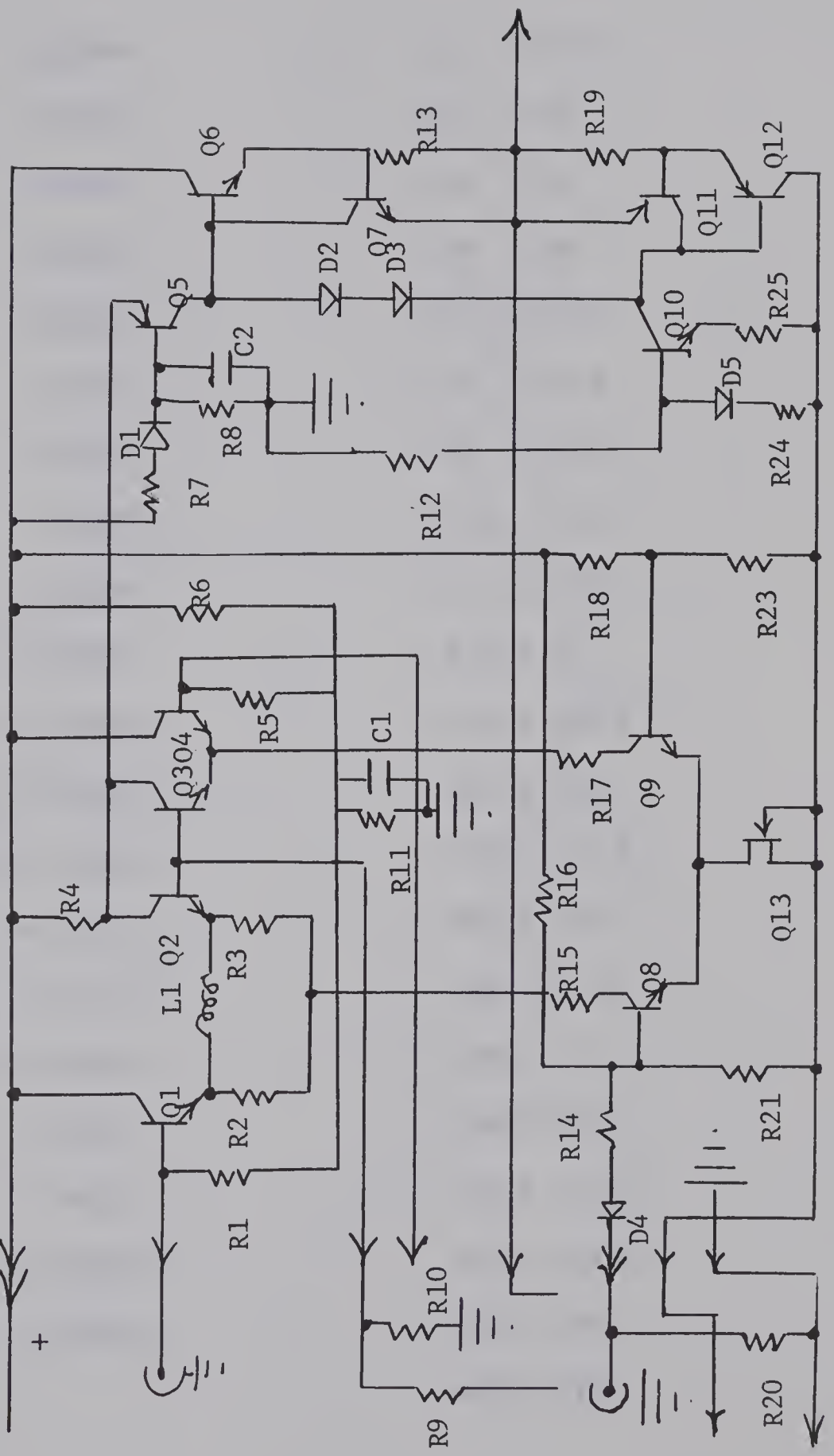

COMPONENT LIST FOR

GATED AMPLIFIER

Q1 = 2N3904

Q2 = 2N3904

Q3 = 2N3904

Q4 = 2N3904

Q5 = 2N3906

Q6 = 2N3904

Q7 = 2N3904

Q8 = 2N3904

Q9 = 2N3904

Q10 = 2N3904

Q 11 = 2N3906

Q12 = 2N3906

Q 13 = 2N3819

C1 = 100 pf

C2 = 250 pf

D1 = BAX13

D2 = BAX13

D3 = BAX14

D4 = 1N4454

D5 = 1N4454

R1 = 12 K

R2 = 56

R3 = 56

R4 = 68

R7 = 270

R8 = 10 K

R9 = 2.2 K

R10 = 2.2 K

R11 = 220

R13 = 11

R14 = 6.8 K

R15 = 330

R16 = 3.3 K

R17 = 330

R18 = 15 K

R19 = 11

R20 = 52 4W

R21 = 3.3 K

R23 = 3.9 K

R24 = 270

R25 = 270

C.3 Transducer drive amplifier

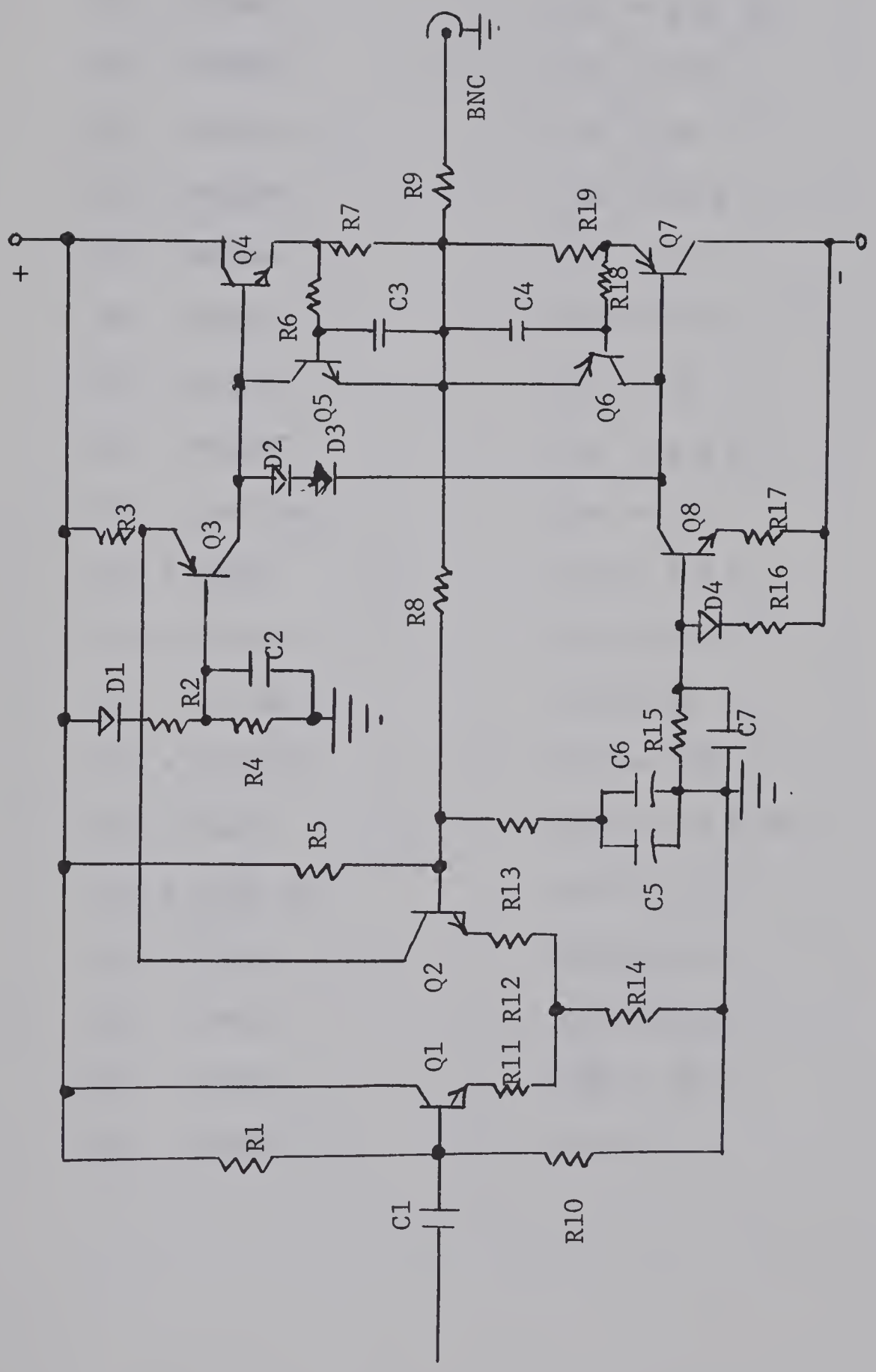

COMPONENT LIST FOR

TRANSDUCER DRIVE AMP

Q1 = MPSH05	R1 = 1 K 1W
Q2 = MPSH05	R2 = 470
Q3 = MPSA56	R3 = 68
Q4 = MPSA06	R4 = 22 K
Q5 = MPSA06	R5 = 1 K
Q6 = MPSA56	R6 = 330
Q7 = MPSA56	R7 = 11
Q8 = MPSA06	R8 = 2.2 K
C1 = .0015 uf.	R9 = 56
C2 = .005	R10 = 2.2 K
C3 = .01 uf	R11 = 68
C4 = .01 uf	R12 = 68
C5 = .003 uf	R13 = 120
C6 = 5 uf	R14 = 1.8 K 2W
C7 = .005 uf	R15 = 22 K
D1 = 1N4454	R16 = 390
D2 = 1N4454	R17 = 100
D3 = 1N4454	R18 = 330
D4 = 1N4454	R19 = 11

C.4 Amplifier and level detector circuit

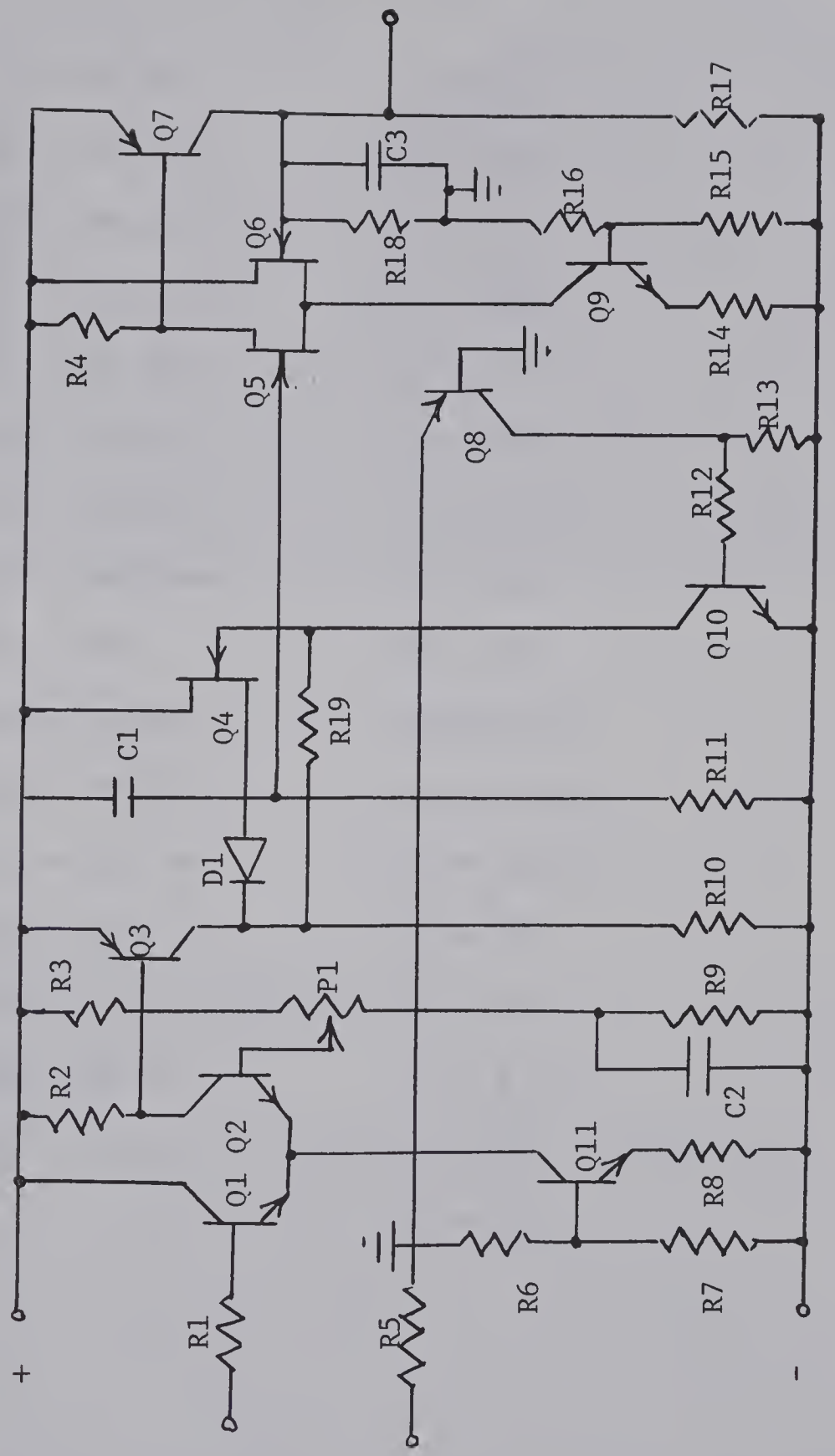

COMPONENT LIST FOR AMPLIFIER

AND LEVEL DETECTOR CIRCUIT

Q1 = 2N 3704	R1 = 1K
Q2 = 2N 3704	R2 = 560
Q3 = 2N 3906	R3 = 1K
Q4 = 2N 3819	R4 = 180
Q5 = 2N 3819	R5 = 12K
Q6 = 2N 3819	R6 = 10K
Q7 = 2N 3702	R7 = 2.2K
Q8 = 2N 3702	R8 = 820
Q9 = 3704	R9 = 1K
Q10= 2N 3704	R10= 1.2K
Q11= 2N 3704	R11= 2.2M
C1 = .005 uf.	R]2= 100K
C2 = .056 uf.	R13= 12K
C3 = 360 pf.	R14= 270
D1 = BAX 13	R15= 2.2K
P1 = 1K pot	R16= 12K
	R17= 12K

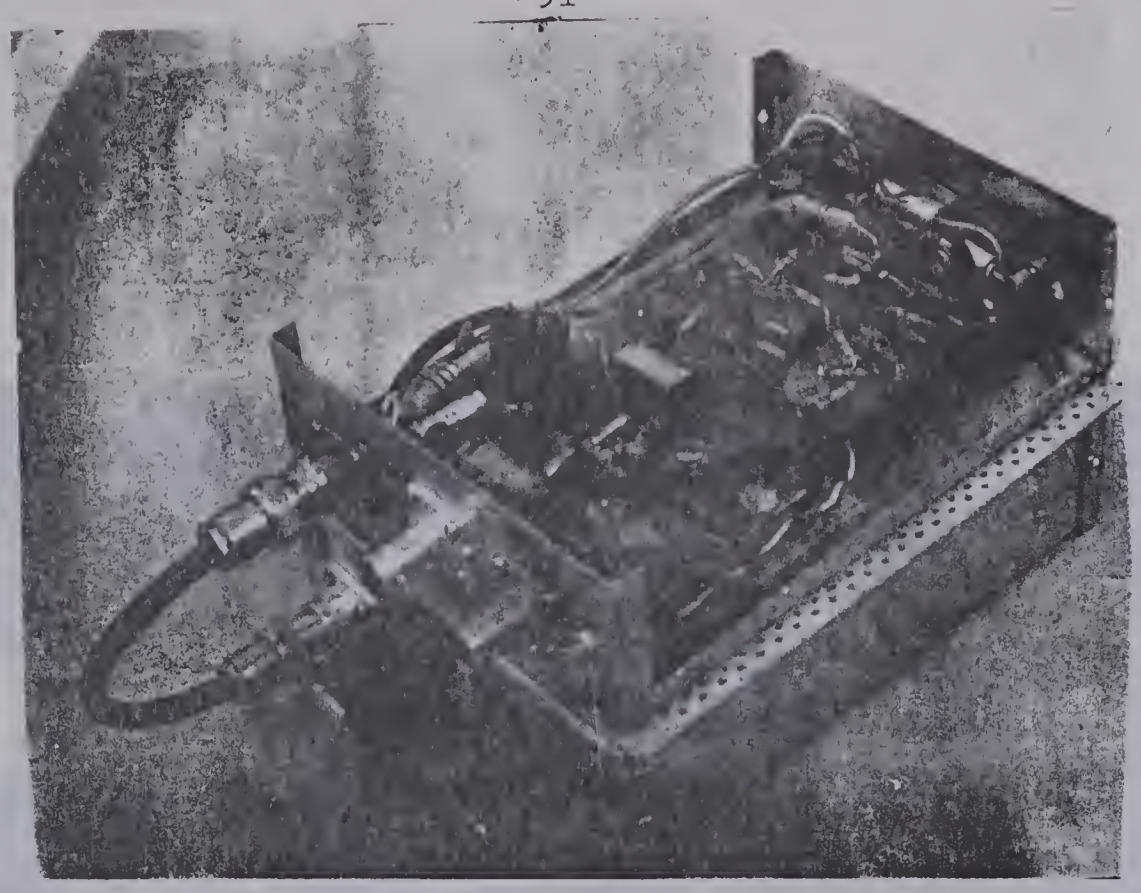

FIGURE 33

Gated amplifier and booster amplifier

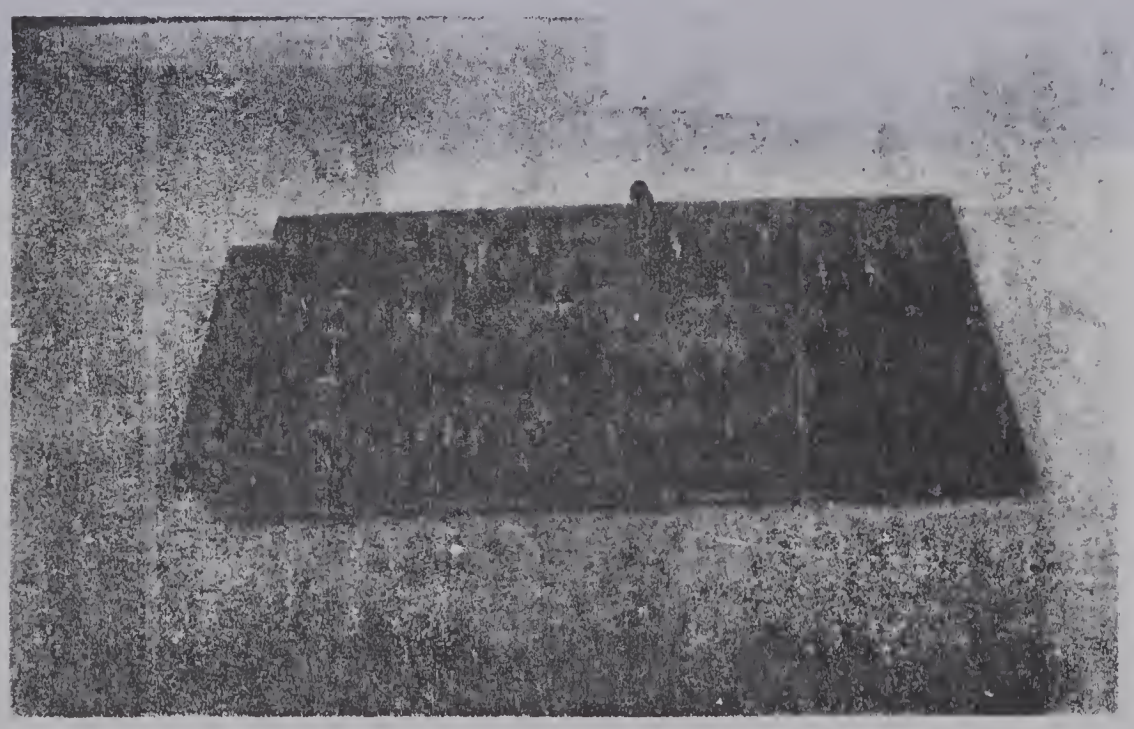

FIGURE 34

Amplifier and level detector

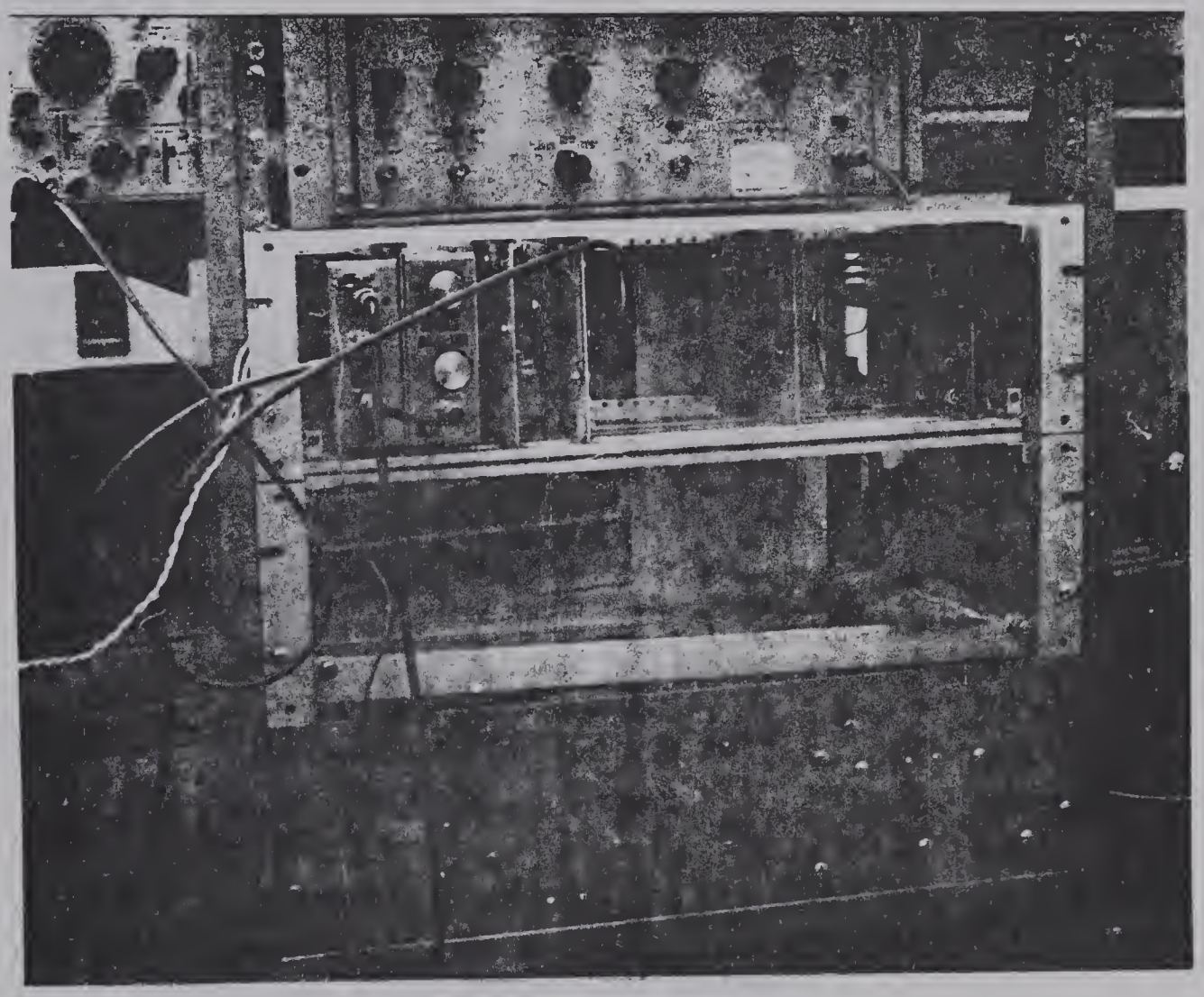

FIGURE 35

Electronics rack

APPENDIX D

PROGRAM TO DETERMINE DIRECTIVITY FUNCTION

```
     ∇ R HPK DTA;PW;PC1;PC;A;X1;X2;F
[1]    RW←R[1]
[2]    RC←P[2]
[3]    R←2↓R
[4]    THTA←DTA[1;]
[5]    AMPN←DTA[2;]
[6]    A←(10((THTA)×(○1÷180)))
[7]    RW←(25.4×P[2]×0.5)÷1.482
[8]    KAW←(○2)×RW
[9]    RC←(25.4×R[2]×0.5)÷1.482
[10]   KAC←(○2)×RC
[11]   X1←(KAW)×(A)
[12]   X2←(KAC)×(A)
[13]   PW←PC←PT←ι I←0
[14] G:I←I+1
15]    1 B1OVERX(X1[I])
[16]   PW←PW,(2×JM)
[17]   1 B1OVERX(X2[I])
[18]   PC←PC,(2×JM)
[19]   →G×ι(ρTHTA)≠I
[20]   I←0
[21] GA:I←I+1
[22]   PC1←F[I]×PC
[23]   PC1←(PC1+PW)÷((⌈/(PC1+PW))
[24]   PT←PT,PC1
[25]   →GA×ι(ρF)≠I
[26]   V←THTA,AMPN,PT
[27]   DTA←KAC←KAW←PC1←PT←PW←P←X1←X2←ι0
[28]   'F IS FRACTION ATTRIBUTED TO COPPER'
[29]   ⎕←F
[30]   ''
[31]   'WATER APPERATURE RADIUS IN LAMBDA   ';RW
[32]   ''
[33]   'COPPER APPERATURE IN LAMBDA   ';RX
[34]   '
              ANGLE MEASURED   AS PER F'
[35]   V←((((ρV)÷(ρTHTA)),(ρTHTA))ρV)
[36]   ⎕V
     ∇
```

The program listed below evaluates the function:

$$\frac{J_1(x)}{x}$$

This program is used within the programs listed in appendices D, E and F.

```
     ∇ M BOVERX X
[1]    K←(0,⍳20)
[2]    JM←+/(((¯1)*K)×((X)*((2×K)))÷((!K)×(!(K+M))×(
       2*(M+(2×K)))))
     ∇
```

APPENDIX E

PROGRAM TO EVALUATE INTERFERENCE PATTERN

```
     ∇ A PHD I
[1]    A1←A[1]
[2]    R←26.64
[3]    PH←AD←⍳0
[4]    A2←A[2]
[5]    A←0.533
[6]    I←I×(○1)÷180
[7]    O←-((40×(○1)÷180)+I)
[8]  START:O←O+I
[9]    L1←(((R×(200))*2)+(((R×(100))-A)*2))*0.5
[10]   L2←(((R×(200))*2)+(((R×(100))+A)*2))*0.5
[11]   TH←((L1-L2)×(○(2÷0.148)))
[12]   AP←(((A1+(A2×(20×TH)))*2)+((A2×(10×TH))*2))*0.5
[13]   1 B1OVERX((○1)×(100))
[14]   APP←JM
[15]   AP←APP×AP
[16]   AD←AD,AP
[17]   PH←PH,O
[18]   →START×⍳O<(40×(○1)÷180)
[19]   PH←PH×180÷(○1)
[20]   AD←AD÷(⌈/AD)
[21]   OUT←((2,(⍴AD))⍴(PH,AD))
[22]   OUT←⍉OUT
     ∇
```

APPENDIX F

PROGRAM WRITTEN TO EVALUATE FREQUENCY VERSUS AMPLITUDE

```
     ∇ R CU LE;AA;B;BB;C;CA;CC;COS;E;ETA;F;FO;FR;K;L;LE;M;N;
       PSI;Q;R;RO;SIN;W;X;Y
[1]    M←0.848×¯1
[2]    F←E←⍳0
[3]    LE←LE×2.54
[4]    C←148100
[5]    FO←1023000
[6]    RO←0.85×R←R×2.54
[7]    L←C÷FO
[8]    K←(○2)÷L
[9]    N←⌈((((((K×K)-(M×M÷4))*0.5)×LE)÷○1)
[10]   LE←N×L÷2
[11]   Q←28
[12]   FN←1020000
[13]   L←Q÷(○2×FN)
[14]   CA←1÷(L×((○2×FN)*2))
[15]   FR←900000
[16] START:FR←FR+(2000)
[17]   K←(W←○2×FR)÷C
[18]   B←((K×K)-(M×M÷4))*0.5
[19]   COS←B÷K
[20]   SIN←M÷(2×K)
[21]   AA←1○(B×LE)
[22]   BB←(COS×(2○(B×LE)))-(SIN×(1○(B×LE)))
[23]   X←((K×RO)*2)÷((((K×RO))*2)+1)
[24]   Y←K×RO÷(((K×RO)*2)+1)
[25]   CC←AA+(Y×BB)
[26]   PSI←1÷((1+(((W×L)-(1÷(W×CA)))*2))*
       0.5)
[27]   ETA←COS×PSI÷(((CC×CC)+(BB×X×X×BB))*
       0.5)
[28]   E←E,ETA
[29]   F←F,FR
[30]   →START×⍳FR<1100000
[31]   VE←((2,⍴E)⍴F,E)
[32]   VE←⍉VE
     ∇
```

APPENDIX H

RADIATION FROM A SIMPLE SOURCE

The velocity potential for a spherical wave is given as:

$$\phi = \frac{A}{r} e^{i(\omega t - kr)}$$

Hence the displacement velocity u is given by:

$$u = -\frac{\partial \phi}{\partial r} = \frac{\phi}{r} + ik\phi$$

p, the partial pressure is given by:

$$p = \frac{\rho_o \partial \phi}{\partial t} = i\omega\rho_o\phi$$

$$Z = \frac{p}{u} = \text{impedance}$$

$$Z = \frac{i\omega\rho_o\phi}{\left(\frac{1}{r} + ik\right)\phi} = \frac{i\omega r\rho_o}{1 + ikr}$$

Now consider a small pulsating sphere of mean radius a. Let the velocity at any point on the surface of the sphere be given by:

$$u_s = U e^{i\omega t}$$

The medium is in contact with the sphere so that at the boundary we have:

$$U\, e^{i\omega t} = \frac{P}{Z}$$

$$U\, e^{i\omega t} = \left[\frac{i\rho_o \omega A}{a}\, e^{i(\omega t - ka)}\right]\left[\frac{ika + 1}{i\rho_o \omega a}\right]$$

If the radius a of the sphere is much smaller than a wavelength then ka << 1 so that:

$$A = \frac{Ua^2}{1 + k^2a^2} = Ua^2$$

Hence:

$$p = \frac{i\rho_o \omega a^2 U}{r}\, e^{i(\omega t - kr)}$$

$$p = \frac{i\rho_o cka^2 U}{r}\, e^{i(\omega t - kr)}$$

Often the partial pressure is written in the form:

$$p = \frac{i\rho_o ck}{4\pi r}\, Q_s\, e^{i(\omega t - kr)}$$

where $Q_s = 4\pi a^2 U$

Q_s is called the source strength and is the maximum volume flow rate of fluid through a surface enclosing the source.

Radiators which are much smaller than a wavelength produce radiation which is spherical. Suppose that the radiator is a small flat disc of area $d\underline{S}$. If this disc is mounted in a baffle so that

radiation is confined to one side of the baffle the source strength of this radiator is given as:

$$Q_s = 2\ \underline{U}.d\underline{S}$$

where "." is the inner product.

The volume flow rate from this source is $\underline{U}.d\underline{S}$. The factor 2 appears because the radiation is confined to one side of the baffle. The partial pressure for this radiator of area $d\underline{S}$ which is much smaller than a wavelength is written as:

$$dp = \frac{i\rho_o ck}{2\pi r}\ e^{i(\omega t - kr)}\ \underline{U}.d\underline{S}$$

REFERENCES

[1] L. D. Rozenberg, Sources Of High Intensity Ultrasound, Vol. 1 Plenum Press, New York, 1969, Introduction.

[2] G. Kossoff, Design Of The C. A. L. Ultrasonic Generator For The Treatment Of Meniere's Disease, IEEE Transactions On Sonics And Ultrasonics, Vol. SU-11, pp. 93-101; 1964.

[3] L. D. Rozenberg, Sources Of HIgh Intensity Ultrasound, Vol. 1 Plenum Press, New York, 1969, Chapter 3.

[4] W. H. Wells, Acoustic Holography, Vol. 2 (A. F. Metherell and L. Larmore, eds.), Plenum Press, New York, 1970, Chapter 8.

[5] H. M. A. El-Sum, Acoustical Holography, J. Opt. Soc. Am., 58 (11): 1548, 1968.

[6] O. K. Manardi, Acoustical Holography, Vol. 2 (A. F. Metherell and L. Larmore, eds.) Plenum Press, New York, 1970.

[7] J. E. Jacobs, Ultrasound Image Converter Systems Utillizing Electron-Scanning Techniques, IEEE Transactions On Sonics And Ultrasonics, SU-15 (3), pp. 146-152, July 1968.

[8] A. Macovski, Hologram Information Capacity, J. Opt. Soc. Am., 60 (1), 1970

[9] I. B. Crandall, Theory Of Vibrating Systems And Sound, D. Van Nostrand Company, 1927, pp. 158-174.

[10] L. E. Kensler and Frey, Fundamentals Of Acoustics, John Wiley and Sons, New York, 1950, pp. 275 - 279.

[11] P.M. Morse, Vibration And Sound, McGraw-Hill, 1948, pp.279 - 281.

[12] L. E. Kensler and Frey, Fundamentals Of Acoustics, John Wiley and Sons, New York, 1950,pp. 163 - 167.

[13] L.E.Kensler and Frey, Fundamentals Of Acoustics, John Wiley and Sons, New York, 1950,pp 177 - 180.

[14] L. E. Kensler and Frey, Fundamentals Of Acoustics, John Wiley and Sons, New York, 1950, pp. 324 - 329.

[15] I. B. Crandall, Theory Of Vibrating Systems And Sound, D. Van Norstrand Company, 1927, pp. 85 - 88; 113 - 115: 153.

[16] R. N. Thurston, Physical Acoustics, Vol. 1 (W. P. Mason, ed.) Academic Press, New York, 1964, pp. 58 - 59.

[17] L. E. Kensler and Frey, Fundamentals Of Acoustics, John Wiley and Sons, New York, 1950, pp. 117.

[18] L. E. Kensler and Frey, Fundamentals Of Acoustics, John Wiley and Sons, New York, 1950, pp. 503.

[19] P. M. Morse, Vibration And Sound, McGraw-Hill, 1948, pp. 265 - 271.

[20] P. M. Morse, Vibration And Sound, McGraw-Hill, 1948, pp. 269.

[21] P. M. Morse, Vibration And Sound, McGraw-Hill, 1948, pp. 271.